TAMPEREEN TEKNILLINEN YLIOPISTO
TAMPERE UNIVERSITY OF TECHNOLOGY

Kimmo Lahtinen

Statistical WVTR Models for Extrusion-Coated Webs in Various Atmospheric Conditions

Julkaisu 880 • Publication 880

Tampere 2010

Tampereen teknillinen yliopisto. Julkaisu 880
Tampere University of Technology. Publication 880

Kimmo Lahtinen

Statistical WVTR Models for Extrusion-Coated Webs in Various Atmospheric Conditions

Thesis for the degree of Doctor of Technology to be presented with due permission for public examination and criticism in Festia Building, Auditorium Pieni Sali 1, at Tampere University of Technology, on the 14th of May 2010, at 12 noon.

Tampereen teknillinen yliopisto - Tampere University of Technology
Tampere 2010

ISBN 978-952-15-2349-6 (printed)
ISBN 978-952-15-2386-1 (PDF)
ISSN 1459-2045

ABSTRACT

The target of this study was to establish statistical prediction models for the water vapour transmission rate (WVTR) of extrusion-coated papers and paperboards commonly used in food packaging. The models bring along reliable and easily available information about materials' moisture barrier, estimate packaging costs and optimise food quality at specific packaging applications. Furthermore, the models can help laboratories to reduce the expenditure of the rather time-consuming WVTR testing.

Another target of the study was to investigate the fundamentals concerning the influences of thermo-hygrometric conditions on the water vapour barrier properties of extrusion-coated webs. Also, the effect of intensive heat treatments (or processes made at elevated temperatures) on the barrier properties were planned to investigate.

The study indicates that experimental data can be used in developing accurate prediction models for WVTR. For non-polar coating polymers, it is possible to establish a comprehensive model that calculates WVTR as a function of the following external factors: temperature, humidity and the multilayer profile of the coating. When the coatings contain a water-sensitive ethylene vinyl alcohol copolymer (EVOH) layer, the WVTR can be predicted indirectly by characterising the resistance effect caused by a non-polar skin layer on EVOH water sorption. In such case, atmospheric conditions were not introduced into the model as variables because of the too complex correlation with WVTR.

According to heat treatment experiments, the over-melting-point treatments considerably improved the water vapour and oxygen barrier properties of polyolefin-coated papers, namely low and high density polyethylenes. The improvement was mainly controlled by the crystallisation kinetics in the coating during a slow cooling period. Chemical reactions in polyethylene were also involved with the treatments above 200°C. Concerning polylactide (PLA) coatings, water vapour barrier properties were already improved at lower temperatures. The heat treatments between 100-150°C were able to reorganise the PLA's crystalline and amorphous regions leading to considerably reduced transmission levels.

PREFACE

This work was carried out at Tampere University of Technology, Paper Converting and Packaging Technology (former Institute of Paper Converting). I wish to express my gratitude to Professor Jurkka Kuusipalo for his guidance and support as a manager and supervisor on this dissertation. I am also grateful to Emeritus Professor Antti Savolainen for employing me almost a decade ago and giving me good advice for the upcoming thesis. I wish to thank all the colleagues at our laboratory for the good and inspirational atmosphere over the last years.

I wish to thank the reviewers of this dissertation, Professor Mikael Hedenqvist from Royal Institute of Technology and PhD Jari Räsänen from Stora Enso, for their important work and constructive criticism. I appreciate the excellent work of my co-authors: Lic.Phil. Sami Kotkamo, MSc (Eng) Tapio Koskinen, MSc (Eng) Sanna Auvinen, PhD Kalle Nättinen and MSc (Tech) Jari Vartiainen. Thanks also to the laboratory assistants Hilkka Koivuniemi-Mäkinen, Krista Näsi and Petri Kuusipalo for their important and invaluable help.

Financial support from the Finnish Ministry of Education is gratefully acknowledged. I especially wish to thank the high standard of PaPSaT (International Doctoral Programme of Pulp and Paper Science and Technology) that helped me to improve the value of this work. The supportive roles of Stora Enso Oyj, UPM Kymmene Oyj, Borealis Polymers Oy, Topas Advanced Polymers, Telko Oy and BASF are also acknowledged with gratitude.

Warm thanks are due to my teams Hikiliikkujat, U.C. Samppi and Streetwise Ry. Special thanks go to my physiotherapist Tuulia Luomala. Most importantly, I wish to thank my parents Anna and Tapio, and my sister Sanna for their whole-hearted support during the years of my studies. And in particular, I wish to extend my deepest thanks to my lovely fiancée Maija for her unconditional love and encouragement.

Tampere, November 2009
Kimmo Lahtinen

LIST OF ORIGINAL PAPERS

This dissertation is based on five peer-reviewed articles, hereafter referred to by their Roman numerals.

I **Influence of Temperature and Mixing Ratio on Water Vapor Barrier of Extrusion-Coated Paper**
Jurkka Kuusipalo and Kimmo Lahtinen
Int'l J. Polym. Anal. Charact. **2005**, Vol. 10, Issue 1-2, Pgs. 71-83.

II **Statistical prediction model for water vapor barrier of extrusion-coated paper**
Kimmo Lahtinen and Jurkka Kuusipalo
Tappi J. **2008**, Vol. 7, Issue 9, Pgs. 8-15.

III **Statistical Model Predicting Water Vapor Transmission Rates of High-Barrier-Coated Papers**
Kimmo Lahtinen and Jurkka Kuusipalo
ANTEC 2009 - Proceedings of the 67th Annual Technical Conference & Exhibition, Chicago, IL, June 22-24. Society of Plastics Engineers, Pgs. 220-224.

IV **Influence of High-Temperature Heat Treatment on Barrier and Functional Properties of Polyolefin-Coated Papers**
Kimmo Lahtinen, Kalle Nättinen and Jari Vartiainen
Polym-Plast. Tech. Eng. **2009**, Vol. 48, Issue 5, Pgs. 561-569.

V **Characterization for Water Vapour Barrier and Heat Sealability Properties of Heat-Treated Paperboard/Polylactide Structure**
Kimmo Lahtinen, Sami Kotkamo, Tapio Koskinen, Sanna Auvinen and Jurkka Kuusipalo
Packag. Technol. Sci. **2009**, Vol. 22, Issue 8, Pgs. 451-460.

AUTHOR'S CONTRIBUTION

I The author provided the literature survey and organised the experimental tests of the study. He also assisted in writing the paper. This paper is based on part of the author's Lic. Tech. thesis work.

II The author organised the study, made the literature survey, provided the calculations and wrote the paper as a corresponding author.

III The author organised the study, made the literature survey, provided the calculations and wrote the paper as a corresponding author.

IV The author organised the study and was the corresponding author of the paper. He looked after the heat treatments and was responsible for the WVTR measurements. The writing regarding these areas and the introduction were contributed by the author.

V The author organised the study and was the corresponding author of the paper. He looked after the heat treatments, was responsible for the WVTR measurements and provided the WVTR equations. The writing regarding these areas and the introduction were contributed by the author.

The research reported in this thesis was carried out under the supervision of Professor Jurkka Kuusipalo.

ABBREVIATIONS AND SYMBOLS

ATR	attenuated total reflection
bw	basis weight
COC	cyclo-olefin copolymer
cw	coating weight
DSC	differential scanning calorimetry
ERH	equilibrium relative humidity
EVOH	ethylene vinyl alcohol copolymer
FTIR	fourier transform infrared
HDPE	high density polyethylene
IR	infrared
LDPE	low density polyethylene
MAH	maleic anhydride
MD	molecular dynamics
O_2TR	oxygen transmission rate
PA	polyamide
PE	polyethylene
PLA	polylactide
PP	polypropylene
PVOH	polyvinyl alcohol
RH	relative humidity
SBS	solid bleached sulphate
stdev	standard deviation
tie	tie layer
TSA	transition-state approach
TUT	Tampere University of Technology
WVTR	water vapour transmission rate

A	area
a_w	water activity
β	tortuosity factor
c	concentration
D	diffusion coefficient
E_d	activation energy of diffusion
E_p	activation energy of permeation
ϕ	relative humidity
L and l	thickness
λ^2	mean square of jump distance
ΔH	heat of solution
J	diffusion coefficient
m	mass
M	molecular weight
ϖ	mixing ratio
p	pressure
P	permeability coefficient
Q	mass of penetrant
R	resistance term (Chapter 4.5)
R	gas constant
R^2	coefficient of determination
S	solubility coefficient
t	time
T	temperature
T_g	glass transition temperature
T_m	melt temperature
τ	immobilisation factor
ν	average jump frequency

TABLE OF CONTENTS

1. THE AIM OF THE STUDY

The scope of this study can be divided into two categories:

1) Statistical modelling of water vapour barrier properties for extrusion-coated webs
2) Influence of heat treatments on water vapour barrier of extrusion-coated webs

In general terms, the papers **I**-**III** cover the research for the first category while papers **IV** and **V** deal with the influence of heat treatments. Nevertheless, all the articles include elements from both of these categories.

One of the most decisive factors affecting shelf life of packed foods is the moisture exchange between the package and the surrounding atmosphere. In general, packaged foods will lose or gain water until the humidity inside the package achieves the food's equilibrium relative humidity (ERH), often expressed as water activity, a_w /1/. The moisture exchange between the package and surroundings is typically controlled by choosing the correct materials and amounts of material for the packaging. Common standard test methods are available for laboratories to measure water vapour barrier properties of these materials /2/. However, the measuring of water vapour transmission rate (WVTR) can be costly and time-consuming for laboratories. In order to reduce costs and time, the aim of this study was to create a practical, fast and easy-to-use tool to predict WVTR. Regarding the development of new packaging materials, the tool could help in material selection, cost estimation and optimisation of the new structures. Also, when the barrier information is needed at diverging conditions, the tool could deliver beyond the range of experimental devices.

There are plenty of sophisticated models already available for the prediction of substance diffusion in polymers /3/. However, the packaging sector, willing to reduce its expenses, does not have much interest to replace experimental testing with less precise and, still, expensive theoretical simulations /3/. Ultimately, permeability of polymers (also in extrusion-coated structures) is a complex process including many sources of variation. This variation is prone to make the modelling and simulation of the permeation process difficult

and expensive. To overcome the problem of complexity, the barrier simulations in this study are made for the actual WVTR value. The WVTR is predicted as a function of external factors, namely the thickness profile of the multilayer coating and the temperature and humidity of surrounding atmosphere. Being independent of processing conditions, these factors are present in all extrusion-coated paper and paperboard products. The polymer-dependent factors influenced by complex phenomena are not neglected, but embedded in the models making them reliable but also rather case-sensitive.

The mechanical properties required for the packages made of extrusion-coated paper or paperboard are mainly governed by the used substrate. Therefore, comparing to film industry, the function of the polymer coating can be aimed towards its primary task: to form sufficient barrier properties for the packaging material. Most extrusion coatings are manufactured at relatively high temperatures that are necessary for gaining adhesion with the substrate. After the materials are attached, the film is rapidly quenched in order to avoid blocking at the laminator. The rapid quenching from such high temperatures solidifies the polymer and stops the crystallisation and packing processes leading to a relatively loose polymer structure with low degree of crystallinity.

By heating the coatings to high temperatures and cooling them slowly back to room temperature, the target of the study was to change the morphology of the rapidly quenched coating via reorganised polymer chain crystallisation and packing processes. The purpose was to improve the barrier properties of the coating without compromising too much from the other important properties of the material. If improved barrier properties were found, the heat treatments could be used as a post-processing method for extrusion-coated webs enabling the use of decreased coating weights and opening new applications for the materials.

2. INTRODUCTION

2.1. Permeability of polymers

Extrusion coating polymers are usually semi-crystalline materials consisting of tensely packed, impermeable crystallites and non-ordered, permeable amorphous sections. Some totally amorphous polymers are also available. Because of the availability and mobility of free volume within amorphous sections of polymers, polymer films have the ability to dissolve molecular species and to allow the transport of these molecules through solid phase. Polymers allow the passage of small molecular species such as carbon dioxide, oxygen, nitrogen and water, while restricting the transport of structurally larger organic molecules. /4-6/

Permeability of polymers is usually expressed as permeability coefficient, *P* (a.k.a. permeability constant or permeability). Generally, permeability coefficient is a proportionality constant between the volume flow of penetrant per unit area of membrane per unit time and the driving force per unit thickness of membrane. Applying this approach, the unit of permeability coefficient is introduced in Equation (1). In literature, on the other hand, different units of transport are considered as units of permeability. Therefore, it is advisable to look carefully at the units when searching permeability information. /7,8/

$$\frac{(\text{amount of gas})(\text{thickness of membrane})}{(\text{membrane area})(\text{time})(\text{differential pressure of gas})} = \frac{cm^3 * mm}{m^2 * day * atm} \qquad (1)$$

Permeation of molecules through polymer films can be a consequence of several mechanisms. Concerning the transport of relatively small molecules, at least three processes occur: i) flow through pores or pinholes in the membrane, ii) diffusive flux of molecules dissolved in the membrane and iii) concurrent operation of the above mechanisms /7/. The combined process has been studied in detail by Frisch /9/.

Regarding the permeation through pores or capillaries of a membrane, the controlling factors governing permeability are size of the penetrating molecules relative to pore and the viscosity of the penetrant. The driving force for such permeation is always the pressure drop across the membrane regardless of the phase of the penetrant. The theory of flow through porous media is elaborated in /7/. In extrusion coating, the pinholes passing through the whole thickness of the coating typically disappear when using coating weights above 10-15 g/m^2 /10/. If the pinholes do not penetrate the whole film thickness, their influence on total permeability remains relatively small /11/.

The following section shows the basic principles of diffusion concerning dissolved molecules in polymer membranes. The introduced description is a generalisation of the sometimes complex permeation process but can be used as a frame of reference in the investigations of this work.

2.2. Activated diffusion

In a polymer film, which has no pores or voids, the permeation of small molecules occurs via activated diffusion process. In activated diffusion, the transport of small molecules is a three-stage process including /7,12-16/:

1) sorption of the penetrant onto the polymer,
2) diffusion of the penetrant through polymer matrix along the concentration gradient, and
3) desorption of the penetrant from the opposite side of the film.

The driving force for the activated diffusion is always the tendency to equalise the chemical potential of the penetrant in the phases separated by the polymer film. In most cases, the chemical potential can be expressed in terms of concentration and pressure /12,15/.

If the boundary conditions on both sides of the membrane are maintained constant, steady-state diffusion will be reached after a relatively short build-up period. In steady-state diffusion through an isotropic material the speed of diffusion can be described by the Fick's first law /7,12-16/ which states that

$$J = -D\frac{dc}{dx} \tag{2}$$

where J is diffusion flow through unit area of film, D is diffusion coefficient, c is concentration of the penetrant and x is distance of the sight level from the film's surface having higher penetrant concentration.

Whenever D is independent of c, the equation of Fick's law can be integrated across the thickness of the film to give

$$J_s = \frac{D(c_1 - c_0)}{l} \tag{3}$$

where c_1 and c_0 are the concentrations of the penetrant at the high and low concentration faces of the film and l is the film thickness. At low penetrant concentrations the pressures or partial pressures of the penetrant above the faces of the film are related to concentrations by Henry's law which states that

$$c = Sp \tag{4}$$

where S is solubility coefficient and p is pressure. By combining the Equations (3) and (4), the concentrations c_1 and c_0 can be replaced with pressures p_1 and p_0 in the diffusion flow equation giving /7,12-16/

$$J_s = \frac{DS(p_1 - p_0)}{l}. \tag{5}$$

The product *DS* is equivalent to the permeability coefficient, *P*. Thus,

$$P = DS \tag{6}$$

and

$$J_s = \frac{P(p_1 - p_0)}{l} . \tag{7}$$

Equation (7) is now in the form of the determination of water vapour transmission rate, *WVTR* (g/m^2/24h), which is measured in constant atmospheric conditions. Equation (8) introduces the determination of WVTR, where Q = mass of the penetrant passing through the film, t = permeating time, L = thickness of film, P = coefficient of permeability, A = area of the film and p_2-p_1 = partial pressure difference between the films surfaces. /17/

$$WVTR = \frac{1}{A}\frac{dQ}{dt} = \frac{P(p_2 - p_1)}{L} \tag{8}$$

The equation (6) which illustrates the diffusion and solution dependence of permeability is considered an empirical relationship valid only in ideal conditions. In virtually all polymers, permeation of molecules is controlled by both diffusivity and solubility. The diffusion coefficient, *D*, is a kinetic term that describes the speed of movement. The solubility coefficient, *S*, is a thermodynamic term that describes the amount of penetrant that will dissolve in the polymer. As a consequence, a polymer can have good barrier properties against permeating species because it has low *D* or low *S* or both. /15/

2.3. Factors affecting polymer barrier

Several factors influence the barrier properties of polymers /7,12,18/. The factors can be either dependent or independent of the polymer concerned. Typically, the influences of

polymer-dependent factors such as crystallinity, orientation, molecular weight and chain-to-chain bonding are complex and difficult to interpret. While their principles are well known, the magnitude of changes caused by them can differ remarkably depending on the case. In addition, even if the properties of the used polymer are well studied and understood, each fabrication process brings its own impact on the barrier properties, e.g. via unique shear and heating faced by the polymer at the extruder or faster/slower quenching faced by the film at the laminator.

There are specific factors in polymer matrices that lead to good barrier properties. Very often these factors define the barrier against one or a couple of permeating species, such as permanent gases (O_2, N_2 etc.) or condensable vapours (H_2O etc.) /15/. For example, polar polymers such as polyamide (PA) and polyvinyl alcohol (PVOH) have good gas barrier properties because of their strong intermolecular bonding but they are poor barriers against water due to the high water sorption. Conversely, very non-polar hydrocarbon polymers such as polyethylene (PE) have good barrier properties against water but poor ones against permanent gases due to the very little cohesion between polymer chains. In general, the following properties of polymers are helpful in obtaining good barrier properties against penetrants:

- certain degree of polarity
- high chain stiffness
- inertness
- close chain-to-chain packing by symmetry, order, crystallinity or orientation
- some bonding or attraction between chains
- high glass transition temperature /19/.

2.3.1. Influence of temperature, humidity and layer thickness

The factors affecting polymer barrier are sometimes independent of polymer (external factors). These factors include temperature and humidity of the surrounding atmosphere,

and the composition of the gas or vapour permeating through the polymer. The thickness of the polymer film or the layer profile of the film can be added to the list because their influence derives from the “amount of polymer”, not from the “quality of polymer”.

If permeation occurs via activated diffusion, the thickness of the polymer layer is inversely proportional to the diffusion flow as shown in Equation (7). This is a commonly used generalisation also applied in this study /7/.

The influence of temperature on diffusion, solubility and permeability coefficients is described by Arrhenius type equations /7,12/. The equations state that

$$P = P_0 \exp\left(-E_p / RT\right) \tag{9}$$

$$D = D_0 \exp\left(-E_d / RT\right) \tag{10}$$

$$S = S_0 \exp\left(-\Delta H / RT\right) \tag{11}$$

where E_d and E_p are the activation energies of diffusion and permeation, respectively, ΔH is the heat of solution of the penetrant in the polymer, R is a gas constant and T is temperature in Kelvin scale. The activation energies and the heat of solution are connected to one another as follows:

$$E_p = \Delta H + E_d \,. \tag{12}$$

The sorption of a penetrant in a polymer can be divided into two processes: condensation and mixing. Thus, the heat of solution can be expressed as a sum of condensation and mixing components:

$$\Delta H = \Delta H_{cond} + \Delta H_{mix} \,. \tag{13}$$

For permanent gases (O_2, N_2, etc.), ΔH_{cond} is negligible, i.e. the heat of solution is a positive quantity which is largely described by ΔH_{mix}. For condensable vapours (e.g. H_2O), the heat

of solution is negative because of the large ΔH_{cond}. In such case, the solubility coefficient tends to decrease with increasing temperature. Regarding permeability coefficient, ΔH is usually smaller than E_d which is always a positive quantity. Thus, the permeability coefficient increases with increasing temperature. Nevertheless, in some cases (e.g. water in polystyrene), the negative ΔH nearly equals the E_d of opposite sign. This results in a permeability coefficient nearly independent of temperature. /7/

Regarding water vapour transport, the humidity of surrounding atmosphere is the actual driving force for the permeation process in polymers. According to Equation (8), the moisture's partial pressure difference between the film's surfaces directly affects the WVTR heedless of permeability coefficient. In addition, the permeability coefficient can be affected by humidity. The extent to which a polymer will absorb water vapour depends on the closeness of chemical constitution in the polymer. When the penetrant has a similar polarity as the polymer, a greater amount of penetrant is dissolved. Under these circumstances both the solubility and diffusion coefficients of polymer are likely to increase as a function of penetrant concentration. /7,20,21/

2.4. Permeability of multilayer structures

Consider a polymer laminate consisting of n layers. Denote the thickness of the *i*th layer L_i and its permeability constant P_i. Assuming that every P_i is pressure independent and steady-state flow is present, the total barrier performance of the structure can be estimated with the help of Equation (14). /11,18/

$$\frac{L_{tot}}{P_{tot}} = \sum_{i=1}^{n} \frac{L_i}{P_i} = \frac{L_1}{P_1} + \frac{L_2}{P_2} + \ldots + \frac{L_n}{P_n} \qquad (14)$$

The quantity L_i/P_i, also called as "permeance", can be introduced into the WVTR equation (Equation (8)). Thus, the total WVTR of a multilayer structure can be calculated with the help of individual layers as follows:

$$\frac{1}{WVTR_{tot}} = \sum_{i=1}^{n} \frac{1}{WVTR_i} = \frac{1}{WVTR_1} + \frac{1}{WVTR_2} + ... + \frac{1}{WVTR_n}. \qquad (15)$$

Equation (15) means that the WVTR of a multilayer structure is the same regardless of the order in which the individual layers are assembled. This result follows from the assumption that all the permeability coefficients of the layers are independent of the partial pressure of moisture. If pressure-dependent permeability coefficients are involved, Equation (15) is no longer valid. The layers having moisture-dependent permeability coefficients are typically covered with non-polar layers in order to improve their barrier effects.

Extrusion-coated papers and paperboards can also be considered as multilayer barrier structures in which the barrier properties are mainly controlled by the coating layer. The relatively permeable web material brings also its own impact on the barrier properties. Stannett et al. /11/ studied permeabilities of polyethylene-coated papers and found that papers have very large permeability coefficients comparing to the coating. For all normal coating thicknesses, the rate of permeation was almost entirely governed by polyethylene. This principle was also verified in the case of water vapour transport. Nevertheless, the role of paper should not be neglected too easily. There is no proof that paper will not affect the permeability of the structure when using coating polymers with poorer barrier properties than those of polyethylene. The web material may also cause indirect influences on the barrier properties via roughness and porosity of the fibric surface. These issues are further discussed in Chapter 4.4 of this work.

2.5. Models for diffusion in polymers

Many types of models are available today for the prediction of diffusion in polymers. This section outlines the existing models and shows their principles regarding the diffusion of small molecular substances.

The existing diffusion models can be divided into two categories illustrating the type and development of the models. The first category, classical models, includes the models that are based on phenomenological considerations. The classical models attempt to analyse specific motions of penetrant molecules and the surrounding polymer chains relative to each other and take into account the pertinent molecular forces acting between them. These so-called “heuristic models” are typically used when explanations are needed for experimental diffusion data and the permeation rates must be predicted beyond the range of experimental measurements. /3/

The second category of diffusion models, computational models, includes so-called “ab initio” computer simulations. Computational models are always based on an appropriate set of scientific first principles that describe the polymer and the penetrant at atomistic level. The diffusion process is simulated by observing the motions of the penetrant polymer system over a certain time-loop. There are expectations that computer simulations will one day become a common tool for predicting the complex diffusion processes in polymers comprehensively. /3/

2.5.1. Classical models

The parameters involved in the development of classical models are often average data on the structural geometry and dimensions of the polymer chains and/or the penetrant molecule. These include length of the polymer chains, chain segment angles, estimated average spacings between the polymer chains, uniformly distributed average free-volumes, penetrant collision parameters, etc. Many times the framework of this average data relies on

macroscopic properties of the polymer such as thermal expansion, compressibility, viscosity and density. In other words, ad hoc (heuristic) assumptions are always present on a certain molecular behaviour of the polymer penetrant system. In conclusion, classical models do not predict the diffusion coefficients as a function of true scientific first principles. However, this is not an obstacle to use these models in specific studies. The mathematical formulae based on classical approach often leads to excellent correlations with experimental data whenever bounded penetrant polymer systems are studied. /3/

An important feature regarding classical diffusion models is the polymer's glass transition temperature, T_g. Generally, different diffusion mechanisms operate in rubbery ($T > T_g$) and glassy ($T < T_g$) polymers. Because of chain motions, rubbery polymers respond rapidly to changes in physical conditions and the penetrant polymer system adjusts quickly to a new equilibrium when a penetrating species is absorbed into the matrix (Fickian behaviour). In glassy polymers, the motion of the chains is not rapid enough to completely homogenise the penetrant's environment and the true equilibrium is not found within the time scale of a common diffusion process. Thus, the diffusion process has much more complex nature in the glassy polymers than in the rubbery ones. /15,22-24/

According to the physico-chemical parameters and mathematical formalism the classical models can be classified into i) molecular models, ii) free-volume models and iii) hybrid models. Although in principle, this classification is valid for both rubbery and glassy polymers, the more detailed and accurate treatments have been made mainly for rubbery polymers because of the more elemental diffusion process. /22,23,25-27/

Molecular models for rubbery polymers

The development of molecular models to describe diffusion in polymers began in late 1930's. The early models /28,29/ were greatly simplified with the mathematical formulae expressing only the dependence of the diffusion activation energy, E_d, on the most common parameters of the penetrant polymer system. Later on, more accurate attempts to correlate

the activation energy with microscopic structural features were performed /30-32/. The main assumption made /30/ was that diffusion of a small penetrant takes place by “jumps” between “holes” or “vacancies” created by the thermal fluctuation of the polymer chains. At this point, the diffusion models allowed semi-predictive calculations to define diffusion coefficients but the procedure was relying on the knowledge of additional parameters such as internal pressure in the polymer and average geometric parameters of the polymer chains. Because of the simplicity of motions assumed and crude methods to estimate structural parameters, these models /32/ could only predict the magnitude of diffusion coefficients with simple penetrants.

The molecular concept was further refined in /33,34/. In this system, the diffusional process consists of two states in the context of assumed polymer chain motions. The oscallitory movement of polymer segments was considered several orders of magnitude slower than the movement of the penetrant molecule. In the “normal” state, the four parallel chains are separated only by the mean intermolecular distance having the penetrant molecule embedded between the chains. In the “activated” state, the polymer chains are separated forming a cylindrical void large enough to allow the movement of the molecule (Figure 1).

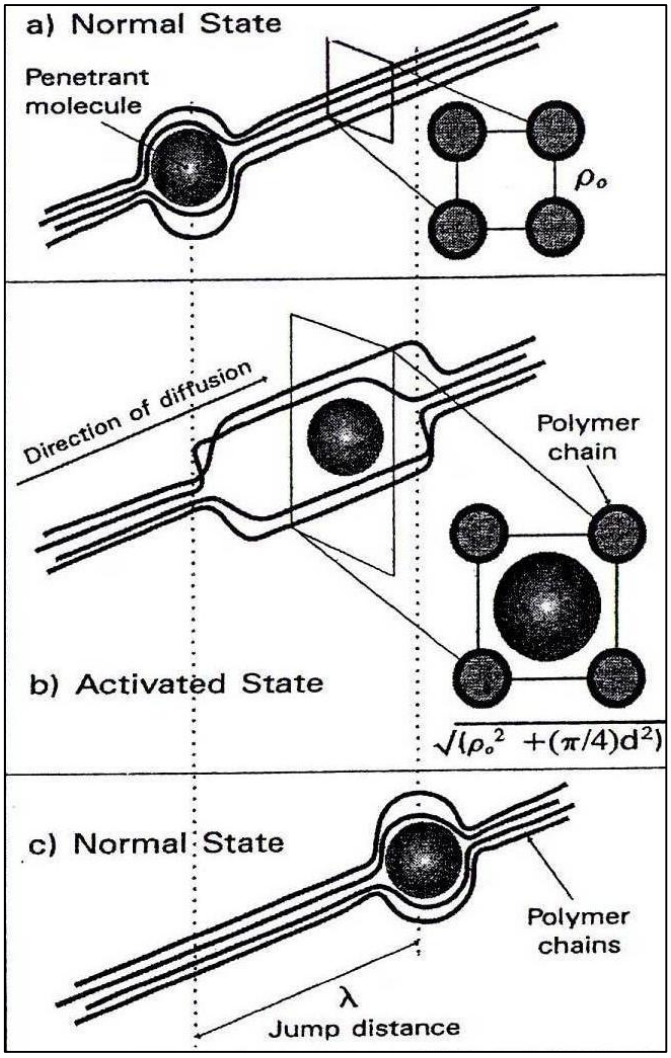

Figure 1. The activation process of diffusion /33/.

One of the most detailed and frequently cited molecular models for the diffusion of simple penetrants in amorphous rubbery polymers was proposed in /35,36/. First, similarly to the systems described in /33,34/, the penetrant model is allowed to move along the axis of a "tube" formed by adjacent parallel chains (longitudinal movement). Second, same way as in /32/, the molecule may move perpendicular to the axis when two parallel chains separate sufficiently to allow the passage (transverse movement). The longitudinal movement was assumed to occur much more rapidly than the transverse. The two motions (Figure 2) occur in series and the observed activation energy, E_d, is required to separate the polymer chains for transverse motion. A detailed discussion on how the equations of this model are used to

analyse diffusion was given in /36,37/. The main advantage of this classical model was that for the first time the E_d could be measured without using any adjustable parameters derived from correlation with experimental data.

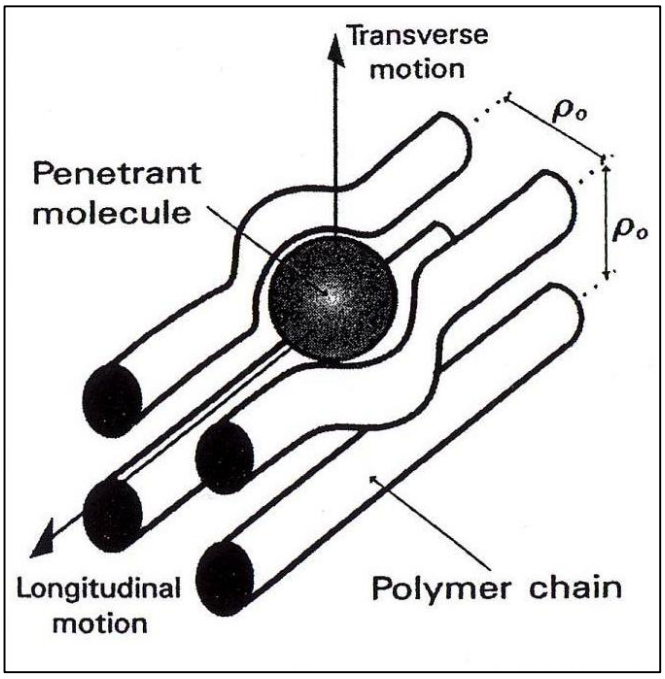

Figure 2. Two motions of spherical penetrant in polymer /3/.

To evaluate the diffusion coefficient *D*, this classical model has to rely on stochastic processes /38/. In a homogeneous polymer matrix, where a penetrant molecule jumps in all directions with equal probability, the diffusion coefficient is calculated with Equation (16).

$$D = \frac{1}{6}\lambda^2 \nu \tag{16}$$

where λ^2 is the mean square of the jump distance and ν the average jump frequency of the penetrating molecule. The difficulty to define λ accurately impairs the usefulness of this model for the type of diffusion estimations important at the packaging sector.

Free-volume models for rubbery polymers

The basic assumption of free-volume models is that the motion of both the polymer segments and the penetrant molecules are determined by the availability of "empty" volume between the chains of the polymer. The phenomenological basis introduced in /39/ has been the starting point for the most free-volume models. In this system, an ideal liquid of hard spheres (molecules) are analysed and confined in a "cage" formed by their immediate neighbours. A fluctuation in density may open a hole within a cage large enough for the displacement of the sphere. This accumulates diffusion when another sphere jumps into the same hole before the first sphere returns back to its initial position. As a result, the redistribution of the free-volume within the spheres ends in a diffusion process which is calculated.

The frequently cited free-volume model by Vrentas, Duda and their co-workers is presented in /40-50/. In order to develop a consistent free-volume model, one must address the following issues: i) how the currently available free-volume for the diffusion process is defined, ii) how this free-volume is distributed among the polymer segments and the penetrant molecules, and iii) how much energy is needed for the redistribution of the free-volume. In all valid free-volume models these issues are addressed from phenomenological and quantitative point of view so that the diffusion process is described adequately down to the microscopic level. It is stated that the model from Vrentas and Duda addresses the requirements so well that it allows the calculation of the diffusion coefficient and the activation energy as a function of parameters with physical significance, i.e. "first principles". The explicit form of this model in a common situation contains fifteen parameters of which thirteen can be determined from thermodynamic and molecular data. These parameters include: two specific hole-free volumes of the components, free-volume parameters for the penetrant and polymer, the thermal expansion coefficient of the polymer, free-volume overlap factors, glass transition temperatures, the fractional composition of the system etc. In general, with the help of a non-linear regression analysis the model is able to calculate the parameters of the theory with only two different diffusivity data points. The

results obtained with this complex procedure have shown good correlation on diffusivity data in several polymer-solvent systems.

The use of free-volume models in the field of packaging, i.e. the diffusion of small substances in polymer films, requires that the selected model is tested for the specific penetrant polymer systems. It is suggested that the free-volume concepts become practical in the future due to the development of computational techniques. /3/

Models for glassy polymers

In glassy polymers, the diffusion behaviour is assumed to be much more complex than that in the rubbery polymers. The diffusion process in glassy polymers can be categorised in three individual cases /51/, i.e. i) the case in which the diffusion process is much slower than the relaxation of the polymer-penetrant system (Fickian diffusion), ii) the case in which the diffusion process is much faster than the relaxation, and iii) the case in which diffusion and relaxation rates are comparable (anomalous diffusion).

Because the free rotation of polymer chains is restricted below T_g it is assumed that fixed microcavities or "holes" of a polymer are "frozen" at these temperatures. Based on this concept, it is suggested that the sorption of simple gases or organic vapour in a glassy polymer has two simultaneous mechanisms: i) dissolution in the polymer matrix according to Henry's law and ii) a hole-filling process according to Langmuir's law. A phenomenological model based on this concept is shown by Equation (17) /52/

$$C = k_D p + \frac{a_1 p}{1 + bp} \qquad (17)$$

where a_1, b and k_D are adjustable coefficients and p and C are the pressure and concentration of the gaseous penetrant, respectively. Because of this dual sorption mechanism the time dependent diffusion equation is much more difficult to define for

glassy polymers than for rubbery ones /53-57/. Also, the parameters of the prediction models are not directly related to the scientific first principles. As a result, exact phenomenological models can only be found in limited cases /55,56,58/. All the other cases need numerical methods in order to correlate experimental results with theoretical estimates. The numerical procedures require a set of starting values for the parameters that are indefinitely guessed. The problem with this approach is that the good correlation may be found with many different starting values making the physical interpretation difficult. However, the mathematical formulae based on the dual sorption mechanism satisfactorily present the dependence of the solubility and diffusivity coefficients for simple gases and organic vapours on the concentration of the penetrant in glassy polymers /15,22-26,59/.

Because local density fluctuations occur in penetrant polymer systems also below T_g, it is reasonable to expect that free-volume models can also provide a description for the diffusion of small molecules in glassy polymers. For this purpose, some of the free-volume models for rubbery polymers have been modified to cover the transport below T_g /43,44,50,60-62/. Also, Vrentas, Duda and their co-workers refined their free-volume model for diffusion in glassy polymers /43,44,61/. In the new model, a series of assumptions on the structure, properties and sample history, and introduction of an additional expansion co-efficient were added to the system. Up to nineteen parameters are needed in this model for the complete description of diffusion coefficient as a function of concentration and temperature. Two of the parameters can be estimated from physico-chemical data available in the literature and the rest of them can be determined from a small amount of experimental diffusion data. It was emphasised that the good correlation between the predictions and experiments could only be obtained with the sample histories similar to the one used in the model.

2.5.2. Computational models

As outlined above, the classical diffusion models often include ad hoc (heuristic) assumptions on certain molecular behaviours of the polymer-penetrant systems. The

conclusion arising from this is that, even if the classical models are able to find excellent correlations to the experimental results, they are not able to predict diffusion coefficient only from the “first principles”. In order to solve this problem, one envisages developing a really atomistic model without any ad hoc assumptions on the molecular behaviour and/or motions in the polymer penetrant systems. Today, the only way to perform this is to simulate theoretically the diffusion process in a polymer matrix by computer calculations.

The construction of a computational model starts by considering an appropriate set of first principles that describe the polymer and the penetrant at a truly atomistic level. This data is then used to create a virtual polymeric structure that has the microscopic and macroscopic properties of a true polymer, i.e. a low energetic state, an appropriate distribution of torsional angles, a distribution of unoccupied volume, density and so on /63-67/. Then, a number of penetrant molecules are randomly inserted into the polymer matrix and the system is left to pursue its molecular dynamics. During this time no heuristic assumptions are made about the molecular dynamics and there is no interference from outside of the system. After a certain time of simulation, the diffusion coefficient can be calculated by observing for example an average displacement of the penetrant species /66/.

The scheme introduced above sounds well-designed but its practical achievement is very difficult. The computer simulation has only lately become a practical approach for the prediction of diffusion coefficients via great computational capacities of new generation computers. For the diffusion of small penetrants (gases, vapours and simple organic substances) in purely amorphous polymers, two computational techniques are available based on molecular dynamics (MD) and transition-state approach (TSA) /68-71/. In semi-crystalline polymers, e.g. a Monte-Carlo 2-phase model can be used for a similar task /72/. So far, MD and TSA techniques are predominantly used to create atomistic diffusion models.

One of the first considerable findings of MD simulation was that in reality the diffusion of small molecules in amorphous polymer matrix occurs in “jumping” motions /73/. Although this is not a new phenomenological finding, the new aspect was that the MD simulation led

to this picture starting from the first principles. In detail, the free volume of a rubbery polymer consists of clearly separated voids with no connection to each other. The penetrant molecule stays confined in one small cavity for a relatively long period of time exploring the cavity thoroughly without being able to exit from it /66,74,75/. This period ends when the molecule leaps quickly from the cavity to another close by as a result of a channel formation. The jump duration is short in comparison to the residence time in a single cavity. Figure 3 shows an example of this "jump" event in a polymer matrix found by a typical MD simulation.

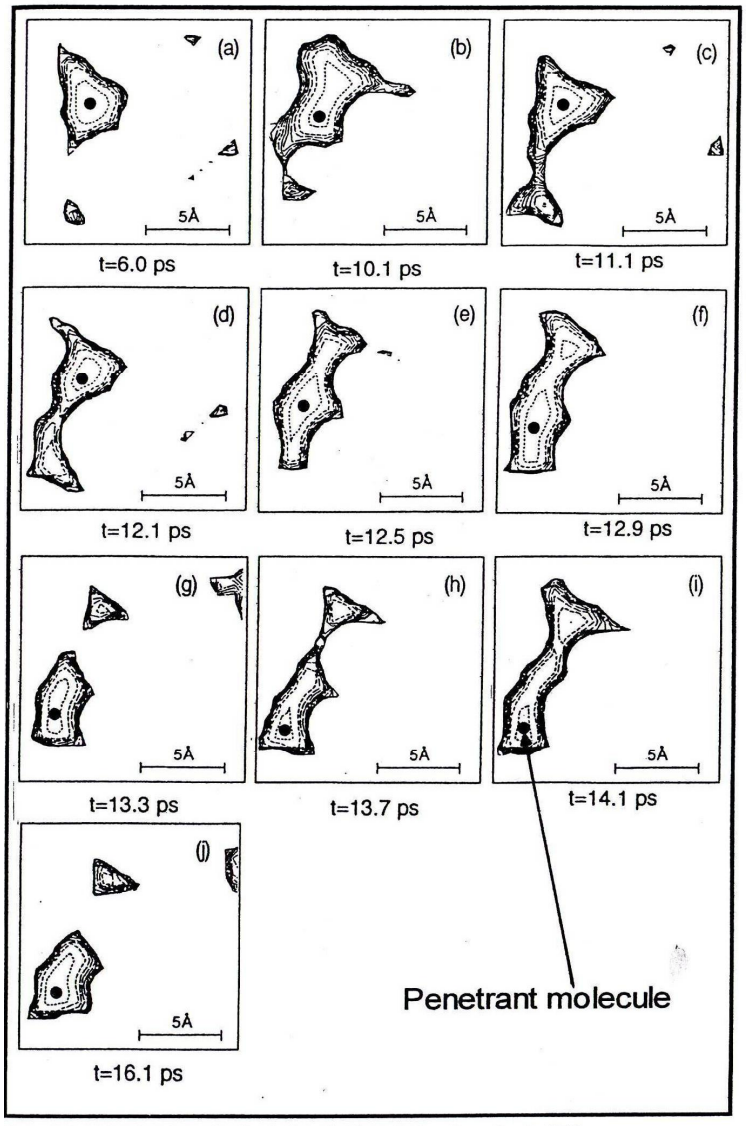

Figure 3. MD simulation of a "jump" of an O_2 molecule /73/.

2.5.3. Usability of diffusion models

The use of prediction models in packaging sector in order to reduce costs and time of laboratories would be of great importance. Nevertheless, the models should meet three basic requirements often set by the packaging industry: i) the model should be as simple as possible, ii) the model should rely on the parameters typical for a specific packaging application and iii) the model should not consume more time and resources than experimental testing. Unfortunately, the prediction models available today do not usually meet all of these requirements. /3/

Practically in all classical diffusion models, one or more adjustable parameters enter in the formula of *D*. To calculate these parameters, a number of diffusion experiments must be performed with the exact penetrant polymer system that one intends to simulate. This requires sophisticated equipment and non-trivial theoretical schemes not commonly used by laboratories. On the other hand, computational models are still under development. The atomistic simulations are available for amorphous polymers but in the packaging sector most of the polymers are semi-crystalline. As regards to future, it is believed that applicable computational methods are available for the prediction of *D* through the development of powerful hardwares. /3/

Several prediction models that estimate transport properties of food packaging materials can be found from literature /76-80/. Some studies have created prediction models also for water vapour transport properties /81-85/. In terms of food deterioration, specific models can be used to investigate shelf life of packed foods /86-90/. Also, many “private” prediction models exist in packaging industry created to fulfil the company’s own demands. It seems that the simplicity and practicability of the models can be improved by developing the models only for specific applications. However, it should be remembered that case-sensitive tools become useless when their limiting values are crossed.

2.6. Influence of crystalline structure on polymer barrier

The thermal history of a polymer and the used processing parameters can be optimised to obtain a structure with improved barrier properties comparing to other structures with same chemistry. When doing this, the crystalline structure of a polymer has an important role. Many polymers used in packaging applications have semi-crystalline structure and, hence, are heterogeneous materials. Because the polymer crystals are practically impermeable, the permeation of low molecular substances occurs through the amorphous phase of the polymer (see Figure 4). /7,12-15,91/

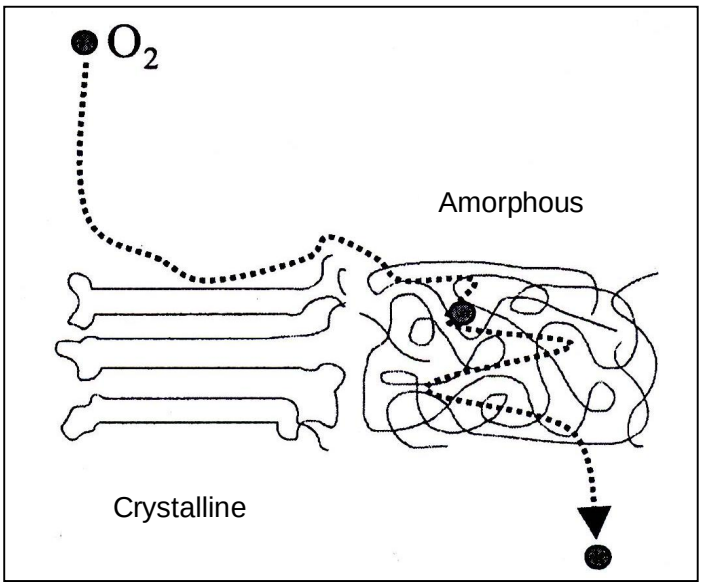

Figure 4. O_2 permeation through the amorphous phase of a polymer /91/.

For mathematical treatment, semi-crystalline polymers can be considered as two-phase systems including a polymer crystalline fraction χ and another fraction in an amorphous state without conformational regularity and lateral order. As the penetrant molecules have to circumvent the crystallites, they are forced to follow a more tortuous diffusion path through the polymer. This effect is accounted in calculations by a so called tortuosity or geometric impedance factor β. The tortuosity factor introduces the path length that the

permeant molecule travels across the film thickness divided by the actual thickness of the film.

The presence of crystals affects also the amorphous phase of a polymer. The segmental mobility of the disordered amorphous fraction is much more restricted in the semi-crystalline polymers than in the fully amorphous ones /92,93/. This effect is taken into account by the so-called chain immobilisation factor τ. With the help of the introduced factors, the effect of crystallinity on the diffusion coefficient can be expressed by using Equation (18).

$$D_{semicrystalline} = \frac{D_{amorphous}}{\beta\tau}(1-\chi) \tag{18}$$

The polymer molecular orientation has also a great influence on the barrier properties of polymers. This is due to i) orientation induced crystallisation, ii) reorganisation of crystals, and iii) reduction of free volume within the amorphous phase of the polymer /91/. The orientation process is able to fractionate and align the crystals perpendicular to the permeant transport causing more tortuous path for molecules to penetrate through the film (increased tortuosity factor). It is also reported that the orientation increases the conformational order of amorphous section, thus, reducing the amount of free volume within polymers. The orientation is also shown to bring the non-equilibrium glassy polymers closer to the equilibrium conditions regarding the transport properties /94/.

Selected studies have investigated the formation of crystalline structure in polyethylenes /95-98/. Neway and his co-workers studied the influence of morphology on polyethylene barrier /99,100/. The properties of polylactide's crystalline and amorphous phases and their influence on barrier properties have also been widely studied /101-104/. These investigations /95-104/ were used as references when the heat treatments of PE and PLA extrusion-coated webs were planned regarding this study.

2.7. Improving the extrusion coating barrier via heat treatments

The polymer density is always lower after extrusion coating than in the unextruded pellet. In extrusion coating, the polymer density is affected by the rate at which the molten film is quenched. Most of this quenching occurs at the chill roll directly after the lamination of the materials. It is, nonetheless, suggested that the quenching does not occur fully at the chill roll. It continues beyond the chill roll due to the retained residual heat of the structure sometimes sufficient to affect the crystallisation of the polymer. In general, selected studies have overviewed the relationship between the processing conditions of polymers and their transport properties /105,106/. In extrusion coating, the coating density and, consequently, the obtained barrier properties are affected by the following process parameters:

- film thickness,
- film temperature immediately after die,
- substrate composition and thickness,
- substrate temperature,
- chill roll temperature,
- chill roll heat transfer properties and
- line speed /107/.

Polymers change their morphological structure when heated to elevated temperatures below the melting point. The heating results in a reorganisation of the structure because the polymer tries to find a state of order that has lower free energy. Two types of structure alterations can occur: irreversible and quasi-reversible changes. These changes depend not only on the temperature but also on the treatment time. Typically, the reversible behaviour occurs when the treatment time is sufficiently short and the irreversible behaviour turns out when the time is further extended. Both types of processes, nevertheless, are observed from majority of heating cases. /108/

The basic irreversible change in heat-treated polymers is the thickening of crystals. This was first observed in late 1950s with solution grown crystals in polyethylene /109,110/ but

occurs also in bulk, melt crystallised and highly drawn samples. In the context of the thickening process, two mechanisms occur simultaneously. Whole crystallites or part of them may melt at elevated temperatures and new crystallites may develop from the amorphous phase at the same time. Molecular weight distribution and crystallisation temperature of the polymer, and the time and temperature of the heating determine which mechanism predominates in the system. It is stated that the partial melting on the surface of crystals plays an important role in the thickening mechanism /108/.

Most extrusion coatings are made at relatively high temperatures in order to obtain better adhesion with the substrate /111,112/. To avoid blocking at the laminator, the hot film is then rapidly quenched at the chill roll unit. The rate of this quenching is typically so high that it freezes the polymer matrix before any advanced crystallisation and packing processes occur leading to a relatively low density of the coating /111/. Sometimes even a totally amorphous structure is achieved for the coating as is the way with PLA coatings /113,**V**/.

By heating the extrusion coating up to high temperatures followed by free cooling at room temperature, it is possible to change the polymer structure for improved barrier properties. The better barrier is achieved as a result of reorganised crystallinity and conformational order of the amorphous phase /114,115/. By using the temperatures below melting point, the crystalline thickening mechanism introduced above is accumulated. With over-melting-point treatments, only the melting mechanism of crystals is available. In such case, the free cooling at room temperature determines the crystalline structure of the polymer.

3. MATERIALS AND METHODS

3.1. Web materials

Four different web materials were used in the study to represent different types of substrates. The materials included two papers and paperboards. Lumiflex 90, a semi-gloss, one-side mineral-coated paper from Stora Enso was used as a substrate in majority of measurements. It provided a smooth and dense web material ensuring even and defect-free coatings for modelling investigations. Swanwhite 83, a bleached kraft paper from UPM-Kymmene, represented a rough and porous paper substrate which was only used for comparative measurements.

Cupforma 210 and 280, solid bleached sulphate (SBS) cup boards from Stora Enso, represented paperboard substrates in the study. Cupforma 210 was used for polylactide coatings in Paper **V** and Cupforma 280 for a comparison study discussed in Chapter 4.4. Table 1 shows the selected properties of the used web materials /116-118/. The Bendtsen roughness values were measured in a laboratory according to standard ISO 8791-3 /119/. The results tabulated in the table are averages of ten parallel measurements.

Table 1. Selected properties of the used web materials /116-119/.

	Grammage (g/m^2) Suppl. data	Thickness (µm) Suppl. data	Roughness top (ml/min) Suppl. data	Roughness top (ml/min) ISO 8791-3	Roughness bottom (ml/min) ISO 8791-3
Lumiflex 90	90	84	12	14	30
Swanwhite 83	83	103	250	265	177
Cupforma 210	210	275	280	-	-
Cupforma 280	280	370	400	403	199

3.2. Coating polymers

Nine different coating polymers were used in the study. Four of them were typical non-polar extrusion coating polymers having good barrier properties against water vapour. Three of the polymers represented polar coatings being good barriers against oxygen but

absorbing moisture when present. The other two polymers were polylactide and anhydride modified LDPE representing a biodegradable coating and an adhesive polymer, respectively. Table 2 shows an overall list of the coating polymers used in the study.

Table 2. Coating polymers used in the study and their supplier informed densities and melting points /120-126/.

Trade name	Polymer	Producer	Density (g/cm^3)	T_m (°C)
CA7230	LDPE	Borealis	0,923	109
CG8410	HDPE	Borealis	0,941	129
WG341C	PP	Borealis	0,910	160
Topas 8007F-400	COC	Topas	1,02	-
EVAL F104B	EVOH	EVAL	1,18	183
Ultramid B27E	PA-6	BASF	1,12-1,15	220
Grilon F 28	PA-6	EMS	1,14	222
Bynel 4288	Mod-LDPE	DuPont	0,92	104
"test grade"	PLA	-	1,25	150-165

3.2.1. Polyethylene

Low density polyethylene (LDPE) is typically used as a heat sealable moisture barrier in extrusion-coated structures. It is still the most common extrusion coating resin used in the world. This highly branched and polydisperse polymer forms a good balance of properties for a product with relatively comfortable processability. The good moisture barrier properties of LDPE are based on the polymer's low polarity. Regarding the transport of oxygen and other non-reactive gases, LDPE has very little cohesion between polymer chains, which leads to high transmission levels. /127,128/

When better abrasion resistance and barrier properties are needed for a coating, LDPE is typically replaced with high density polyethylene (HDPE). HDPE has a denser and less-branched structure, which makes it a slightly better barrier than LDPE. On the other hand, the HDPE processing is more difficult than that of LDPE, and there is still very little cohesion or attraction between the polymer chains needed for good barrier properties against permanent gases. /127,128/

3.2.2. Polypropylene

Polypropylene (PP) finds use in extrusion coating due to its temperature and grease resistance. It can withstand temperatures up to 105°C in continuous use and up to 120-130°C for short periods. PPs are sometimes blended with PE (also WG341C, Table 2) in order to obtain better low-temperature performance and heat sealing properties. PP-homopolymers tend to become brittle at freezing temperatures. /127/

Because of the non-polar nature the moisture barrier properties of PP are more or less equal with polyethylenes. Nonetheless, PP's polymer chains are a little bit stiffer due to the CH_3 groups making the polymer a slightly better barrier against permanent gases. /127/

3.2.3. Cyclo-olefin copolymer

Cyclo-olefin copolymer (COC) refers to amorphous ethylene norbornene copolymers. COCs have properties that are customised by varying the norbornene content of the structure, which affects the glass transition temperature of the polymer (varies from 60 to 180°C). Typically, the low T_g versions of COC are used for extrusion coating purposes. /129-131/

Like other polyolefins, COCs have good barrier properties against moisture but are moderately permeable to atmospheric gases. Generally, COCs have the best barrier properties among polyolefins because they are in a glassy state under normal use conditions. Another advantage of COC is its amorphous structure. The amorphous nature of COC can help with the harmful curling phenomenon often confronted in extrusion coating with semi-crystalline polymers. On the other hand, COCs have poorer adhesion and sealability properties than polyethylenes. /129-131/

3.2.4. Ethylene vinyl alcohol copolymer

Ethylene vinyl alcohol copolymer (EVOH) is used as a grease, oxygen and light barrier in extrusion coating. EVOH is a moisture sensitive material and needs to be sandwiched between hydrophobic skin layers such as PE. Water molecules are able to hydrogen bond with the EVOH hydroxyl groups resulting in plasticisation and swelling of the polymer. Because of the excellent oxygen barrier properties in dry conditions, EVOH is many times considered as a non-metallic alternative to the aluminium foil layer. /132,133/

EVOH's good barrier properties against permanent gases are based on its high crystallinity and high level of hydrogen bonding between the polymer chains. The barrier properties of EVOH are affected by the processing conditions in which the polymer film is re-crystallised and/or oriented. Also, the ethylene content of the polymer affects the barrier properties. As the ethylene content decreases the barrier properties of the film improve, whereas the increased ethylene content leads to improved formability and mechanical properties. Typical ethylene contents of EVOH resins available are 27-48%. The ethylene content of EVAL F104B is 32 mol-%. /123,132,133/

3.2.5. Polyamide

Polyamides (usually type 6 = PA-6) are tough materials with high tensile strength and melting point. PA has moderately good oxygen barrier properties but relatively high water vapour permeability. PA films laminated with PE are typically used for thermoformed packages containing meat, cheese or fish. PA can be coextruded with EVOH without the need of a tie layer. PA's barrier properties are poorer than EVOH's but it has considerably better mechanical properties. The polymer chains of PA are attached via hydrogen bonding between amide groups. These bonds are very sensitive to the presence of water. /134/

3.2.6. Adhesive polymer

The coextrusion of EVOH (or PA) with polyethylene requires a tie layer between them in order to obtain adhesion. This tie layer is usually a maleic anhydride (MAH) modified polyethylene (e.g. Bynel 4288). In this material, the grafting of the functional groups onto the polyethylene chain uses a melt homogenisation with peroxides to form free radicals via chain scission and opening of double bonds. The MAH monomer then grafts itself onto the polymer. A typical anhydride-modified LDPE has 0,5-1,0% of grafted monomer. In coextrusion, covalent or hydrogen bonding is formed between the grafted groups and the polar polymer. The interaction with the PE layer occurs via entanglement and compatibility. /127,135,136/

3.2.7. Polylactide

Polylactide (PLA) is a biodegradable polymer that has gained enormous attention as a replacement of synthetic polymers in the last decade. PLA is an aliphatic polyester derived from corn flour or sugarcanes via condensation of lactic acid or the ring-opening polymerisation of the cyclic lactide dimer. Existing extrusion coating equipments useful for common synthetic polymers can be used for processing of properly tailored PLA grades. In an industrial compost environment, PLA degrades to water and carbon dioxide in about 4 to 6 weeks after a non-toxic lactic acid phase. /137-139/

PLA has better barrier properties against oxygen than PE, but its water vapour barrier is several times poorer. PLA's barrier properties are greatly affected by crystallinity and stereochemical purity of the polymer, and orientation during processing. The polymer chain branching and L:D ratios have no considerable influence on PLA's permeability. Because of the complex stereochemistry and the glassy state under normal use conditions, the permeability properties of PLA are not yet completely characterised. /140-142/

3.3. Pilot line trials

Extrusion coating trials of the study were performed at the pilot-line of TUT/Paper Converting and Packaging Technology. For the production of coextruded structures, the line has four extruders, a five-layer feedblock (Cloeren VG 5-layer Dual Plane Feedblock) and a T-type, 700 mm wide die with inner deckle and encapsulation systems (Cloeren EBR III A). Concerning web handling, the maximum speed of the line is 500 m/min, and the maximum width of the web is 550 mm. In addition to extrusion coating, the line can provide dispersion coating and laminating operations. Figure 5 shows a schematic cross-section figure of the used line.

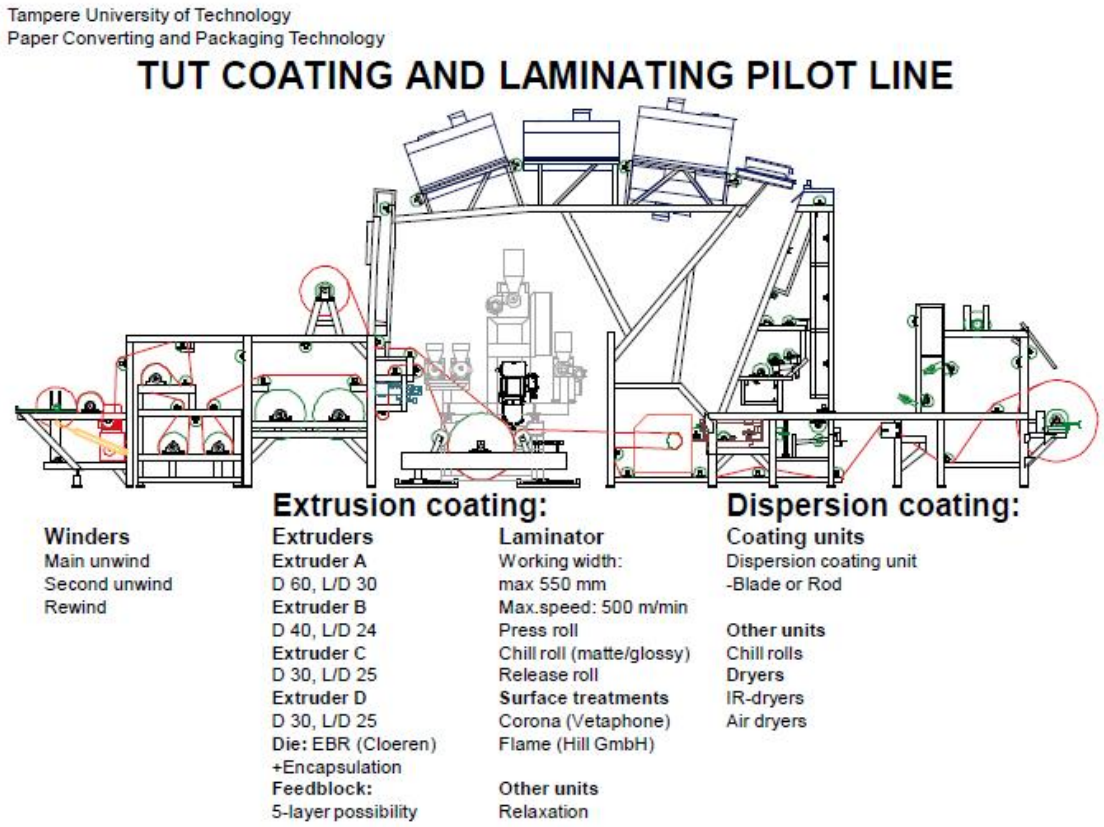

Figure 5. A cross-section figure of the extrusion coating pilot line used in the study.

3.4. Heat treatments

A laboratory convection oven (Firlabo AC 120) was used to provide the heat treatments of the study. The used treatment temperatures varied from 70 to 230°C and the periods from 1 to 40 min.

3.5. WVTR measurements

The WVTR measurements of the study were made according to SCAN P22:68 /143/. The advantage of this traditional "cup method" is its capability to measure a large number of samples simultaneously. This was found useful because of the massive test program scheduled. In the method, a 65 cm^2 circular sample is cut from the middle of a sheet with a standard cutter (Lorentzen & Wettre). The sample is placed against an aluminium dish containing calcium chloride and covered with a cylindrical template having base area of 50 cm^2. Melted wax is poured around the cylinder to seal the sample tightly against the dish. After the wax is cooled, the cylinder is removed and the dish is placed into a controlled atmosphere. After stabilisation, the daily increase in the weight of the dish is measured and converted to WVTR ($g/m^2/24h$).

The wax used in the seams of the dishes was paraffin wax with 12-15% beeswax included. Two conditioning chambers were used in the study. Most of the samples were conditioned in Espec PR-1KPH. Only the PLA-coated paperboard samples of Paper **V** were conditioned in Firlabo SP-BVEHF. The polymer-side of the samples was always exposed to high moisture concentration. Figure 6 shows a series of test specimens in controlled atmosphere during WVTR test.

Figure 6. Aluminium dishes holding a sealed sample in controlled atmosphere.

The prediction models of the study were based on experimental WVTR tests in which the samples were exposed to 16 atmospheric conditions. This was done by forming all the combinations of four temperatures (23, 30, 38 and 45 °C) and four relative humidities (50, 63, 77 and 90% RH) in the conditioning chamber. By producing four sets of samples, each sample went through four conditions. Table 3 shows the conditions used for each series of samples in this procedure.

Table 3. Conditions used in the WVTR test for modelling purposes.

	1. condition	2. condition	3. condition	4. condition
Series 1	23°C 50% RH	30°C 50% RH	38°C 50% RH	45°C 50% RH
Series 2	23°C 63% RH	30°C 63% RH	38°C 63% RH	45°C 63% RH
Series 3	23°C 77% RH	30°C 77% RH	38°C 77% RH	45°C 77% RH
Series 4	23°C 90% RH	30°C 90% RH	38°C 90% RH	45°C 90% RH

3.6. Supportive analytics

Basis weights of web materials and coating weights of extrusion-coated structures were measured from 65 cm^2 circular test samples cut with the same cutter as the WVTR samples. The samples were always cut from the middle of the roll (cross section) in order to avoid errors from neck-in and basis weight variation. The cut sample was weighed with an analytical balance and the result was converted to g/m^2. Coating weight was calculated by subtracting the basis weight of the web material from the result. The subtracted basis weight was always measured from the uncoated areas of the same roll being an average of 10 parallel measurements.

The optical examinations of the study were made with a microscope using magnifications from 4 to 400. Two microscopes, Leitz Diaplam and Zeiss Axioskop 40, were used to examine cross-cut profiles and morphologies of polymers. The morphologies were also studied with an infrared (IR) spectroscope and a differential scanning calorimeter (DSC). IR spectra were studied with Perkin Elmer Spectrum One FT-IR Spectrometer in attenuated total reflection (ATR) mode. DSCs were studied with Mettler Toledo Star DSC821e.

Surface energies of samples were tested with a sessile drop method following the standard ASTM-D 5946 /144/. Two test liquids were used in the test: water and ethylene glycol. The applied equipment was The Pocket Goniometer PG-3. Pinholes of extrusion coatings were studied with a turpentine test in which the test liquid is spread over a coating. After a period of ten minutes, the number of pinholes is counted from the reverse side of the structure from the area of 100 cm^2. The pinholes are observed as coloured spots in the texture.

The oxygen transmission rate (O_2TR) measurements of Paper **IV** were made with Oxygen Permeation Analyser Model 8001 (Systech Instruments) at VTT, Espoo. In this method, the active test area of a sample is 50 cm^2. The coated side of the sample is sealed against test cell using high vacuum grease, thus the paper side is facing oxygen during the measurement. The O_2TR results of the study are mean values of two replicates and expressed as cm^3/m^2/24h.

4. RESULTS AND DISCUSSION

4.1. WVTR calculation model

Coating weight and WVTR values were measured for a comprehensive set of extrusion-coated paper samples having different coating weights. The WVTRs were measured in several atmospheric conditions covering temperatures from 23 to 38°C and relative humidities from 50 to 90%. The individual coating weight and WVTR values were measured from the same test sample so that the results form a dot in xy-scatter in which x equals the coating weight and y the WVTR. As an example, [**I**, Figure 2] shows plotted results for LDPE- and PP-coated papers at 38°C and 90% RH based on 73 and 88 test points, respectively.

According to Equation (8), WVTR is inversely proportional to the thickness (or coating weight) of the barrier layer. Thus, the correlation can be expressed with Equation (19)

$$WVTR = A \times (cw)^{-1} \tag{19}$$

in which cw = coating weight and A = polymer-dependent constant. A more accurate fit was found when the exponent of the equation was unleashed and introduced as constant B also dependent of the polymer (Equation (20)). This procedure was referred to as a power law of regression provided by all the common spreadsheet softwares available.

$$WVTR = A \times (cw)^{B} \tag{20}$$

It was found that samples with only three separate coating weights are needed from trials to define the exponential function for each coating with significant correlation. The chosen coating weights should preferably be 10-15 g/m^2 apart from each other and at least five parallel WVTR measurements should be made for each coating weight. As an example, Figure 7 shows a curve made for COC-coated paper from 5 set points at 30°C, 77% RH.

According to the figure, a strong correlation is found even if slightly inconsistent results are included in the series.

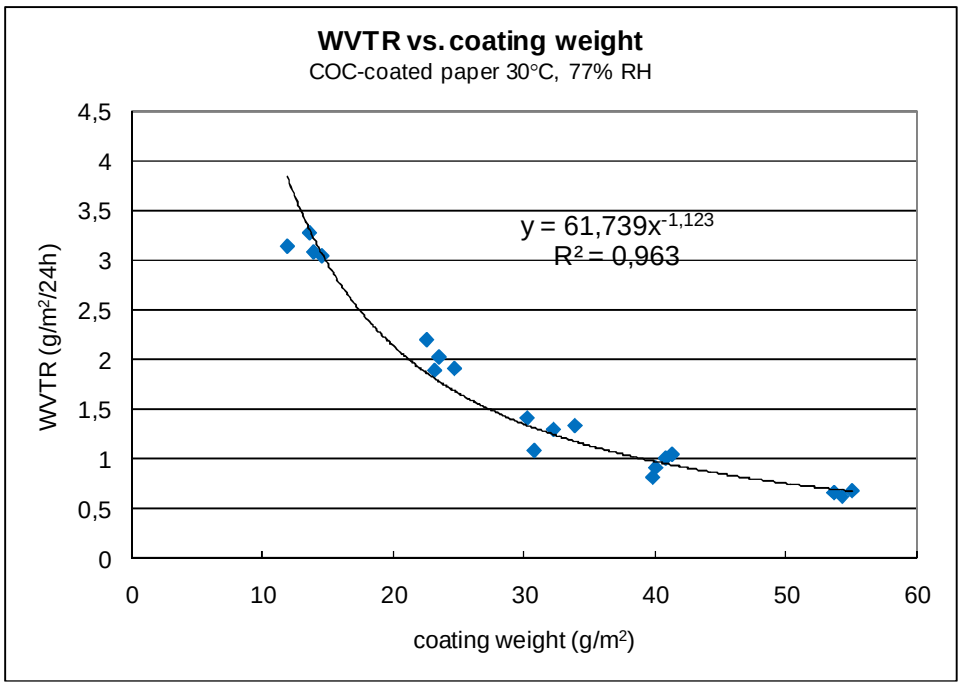

Figure 7. WVTR of COC-coated paper as a function of coating weight at 30°C, 77% RH.

The properties of the introduced WVTR calculation are further discussed in Paper **I**. [**I**, Table 2] shows the exponential equations measured for LDPE- and PP-coated paper. The equations can also be measured for other coating polymers and used for accurate prediction of WVTRs for monolayer-coated webs. To extend the prediction for multilayer coatings, one can apply the theory of permeability for multilayer structures introduced in Chapter 2.4, though, the requirements set by the theory for the independence of pressure and concentration should be taken into account when using this theory. In Chapter 4.3, the exponential equations are used to calculate the WVTRs for an exactly 20 g/m^2 coating weight of each polymer. These values are directly considered as experimental raw data in the established comprehensive model.

4.2. Correlation between WVTR and mixing ratio

The influences of atmospheric conditions, i.e. temperature and humidity, on the WVTR of extrusion-coated papers were also investigated in Paper **I**. One approach was to question the use of relative humidity (RH) as a humidity indicator. Although RH is commonly used in describing humidity conditions, it does not define the absolute water concentration of a certain atmosphere. It only defines the percentage of water mass that would be present in an equal volume of saturated air at a specific temperature. In other words, RH is a temperature-dependent quantity and creates a combined influence on WVTR together with temperature.

To use an independent variable, mixing ratio (a.k.a. specific humidity) was introduced as a replacement of RH. Mixing ratio, ϖ, is defined as the ratio of the amount of water (kg) and the amount of dry air (kg) in the atmosphere /145,146/, i.e.

$$\omega = \frac{m_w}{m_a} \tag{21}$$

where subscripts *w* and *a* denote water vapour and air, respectively. Introducing the perfect gas relation /145/, the ratio of masses changes to

$$\omega = \frac{M_w p_w}{M_a p_a} = 0.622 \frac{p_w}{p_a} = 0.622 \frac{p_w}{p - p_w} \tag{22}$$

where M_w and M_a are the molecular weights of water and air (18.015/28.964 = 0.622), p is normal air pressure = 1 bar, and p_w and p_a are partial pressures of vapour and air at the conditions. Furthermore, the definition of relative humidity (ϕ = RH(%)/100) is

$$\phi = \frac{p_w}{p_w'} \tag{23}$$

where p_w' is saturated vapour pressure. Saturated vapour pressure is a function of temperature and can be found from standard tables of humid air /145,146/. By uniting Equations (22) and (23), mixing ratio can be expressed as a function of relative humidity and temperature as follows /145,146/:

$$\omega = 0.622 \frac{p_w'(T)}{p/\phi - p_w'(T)}. \qquad (24)$$

The behaviour of mixing ratio at different temperatures is illustrated graphically in the Mollier chart (Appendix 1) /146/. It shows the correlations between air temperature, water content and relative humidity. The chart is directly based on Equation (24).

According to test results, mixing ratio has a strong and almost linear correlation with the WVTR of the webs coated with non-polar polymers. Theoretically, this means that the water vapour permeability of such materials is mainly controlled by the difference of the vapour concentrations on the opposite faces of the coating. Temperature influences mainly on the slope of the straight WVTR vs. mixing ratio line which indicates temperature's minor but important role in the permeation process also discussed in Chapter 2.3.1. As an example, Figure 8 shows the WVTR vs. mixing ratio curves drawn for 20 g/m^2 PP-coated paper at different temperatures.

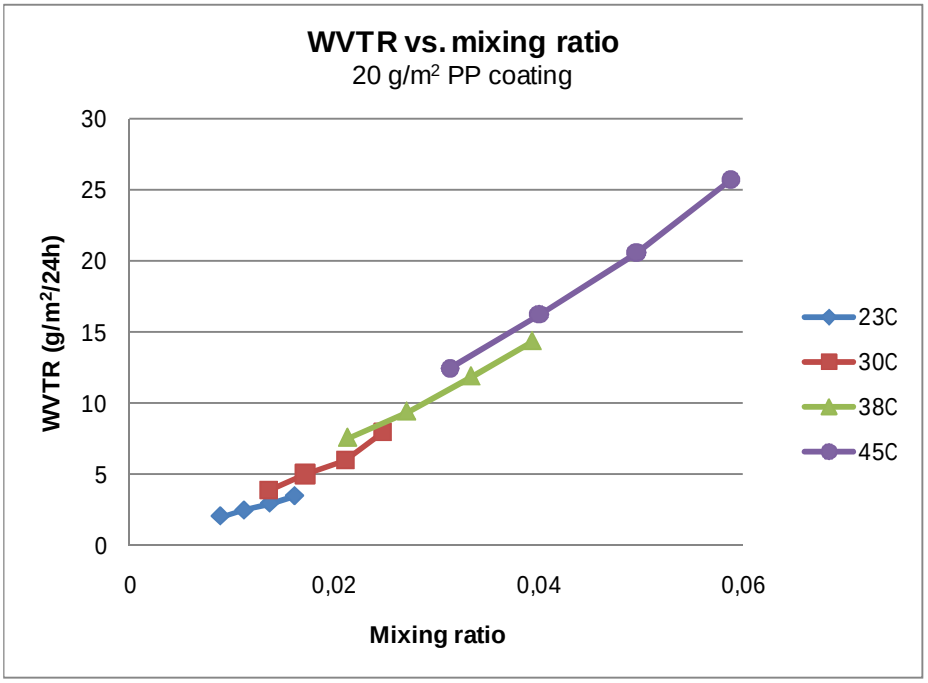

Figure 8. WVTR as a function of mixing ratio for PP-coated paper (coating weight = 20 g/m^2).

With polar coating polymers, the linear correlation between WVTR and mixing ratio was not found. In such cases, the WVTR vs. mixing ratio curve tends to turn left at high RHs, which can be explained by the sorption of water into the polymer followed by increased water vapour transport. Figure 9 shows the WVTR vs. mixing ratio curve measured for 20 g/m^2 EVOH-coated paper.

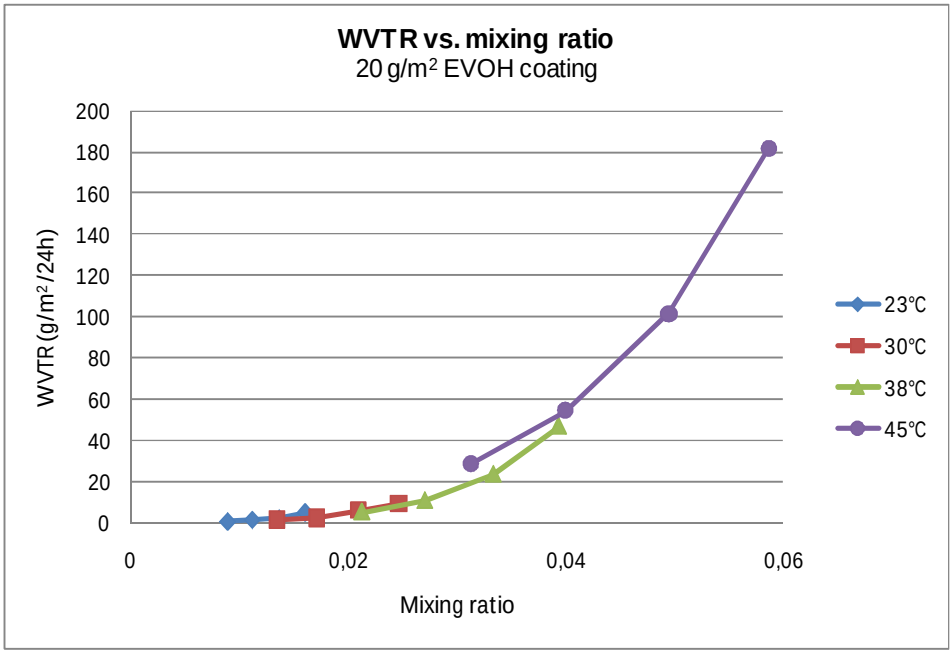

Figure 9. WVTR as a function of mixing ratio for EVOH-coated paper (coating weight = 20 g/m^2).

4.3. Statistical model predicting WVTRs for non-polar coating polymers

A comprehensive statistical model was established that calculates the WVTR of extrusion-coated webs as a function of atmospheric conditions and coating structure. A detailed description of this model can be found from Paper **II**. The model was found applicable only for the coating structures including non-polar polymers. The calculations of the model are based on three steps introduced in Table 4. The modelling is started by estimating the WVTR for a 20 g/m^2 monolayer coating. The best fit is found by using a multivariable model introducing mixing ratio (ϖ) and temperature (T) as independent variables. The model is extended to cover other coating weights and laminate structure in the second and third steps of the calculations, respectively. Equations (25), (26) and (27) show the functions used in the calculations. In the equations, cw equals coating weight and k_{ϖ}, $k_{\varpi,T}$, k_T, A, B and C are constants measured by a statistical software. The subscripts i and 20 denote the layer i of the structure and 20 g/m^2 coating weight, respectively.

Table 4. The basic concept of the model established for non-polar coatings: step-by-step scheme for calculations.

Input	Action	Output
Step 1) The influence of - Temperature - Humidity	Regression model	WVTR of a 20 g/m^2 coating
Step 2) The influence of - Coating weight	Equation: Fick's first law	WVTR of a single layer coating
Step 3) The influence of - Layered structure	Equation: The theory of permeability for multilayer structures	**WVTR of a total structure**

$$WVTR_{i,20}(\varpi,T) = k_{\omega}\varpi^2 + k_{\varpi,T}(\varpi \times T) + k_T T^2 + A \times \varpi + B \times T + C \quad (25)$$

$$WVTR_i(\varpi,T,cw) = \frac{20}{cw_i}\left(WVTR_{i,20}(\varpi,T)\right) \quad (26)$$

$$WVTR_{TOT} = \left[\sum_{i=1}^{n}\left(\left(\frac{20}{cw_i}WVTR_{i,20}(\varpi,T)\right)^{-1}\right)\right]^{-1} \quad (27)$$

Table 5 shows a list of the best fitted $WVTR_{i,20}(\varpi,T)$ functions found for the coating polymers in this research. The reliability indicators (R^2) of the models are also included in the table. Figure 10a illustrates the relationship between the variables in the models. It shows a 3-D surface based on the model for 20 g/m^2 LDPE coating. The 16 experimental data points used in the calculations are also shown in the figure. In comparison, Figure 10b shows a corresponding surface using RH as a variable of humidity. The surface of Figure 10b is not based on the model but drawn based on the experimental data via distance weighted least squares. Figure 10a shows the strong correlation between WVTR and mixing ratio found for LDPE and other non-polar coatings in Chapter 4.2.

Table 5. The best fitted $WVTR_{i,20}(\varpi,T)$ functions (Equation 25) for the LDPE, HDPE, PP and COC coatings of the study.

Constant	LDPE (CA7230) $R^2 = 0,9992$	HDPE (CG8410) $R^2 = 0,9995$	PP (WG341C) $R^2 = 0,9992$	COC (8007F-400) $R^2 = 0,9901$
k_{ϖ}	5101,533	4119,016	3357,386	2832,088
$k_{\varpi,T}$	-	-2,98768	-	-
k_T	-0,00454	-	0,002395	0,000303
A	203,7565	260,9171	178,862	-
B	0,427809	0,149953	-	-
C	-6,94931	-3,57886	-1,23101	0,580239

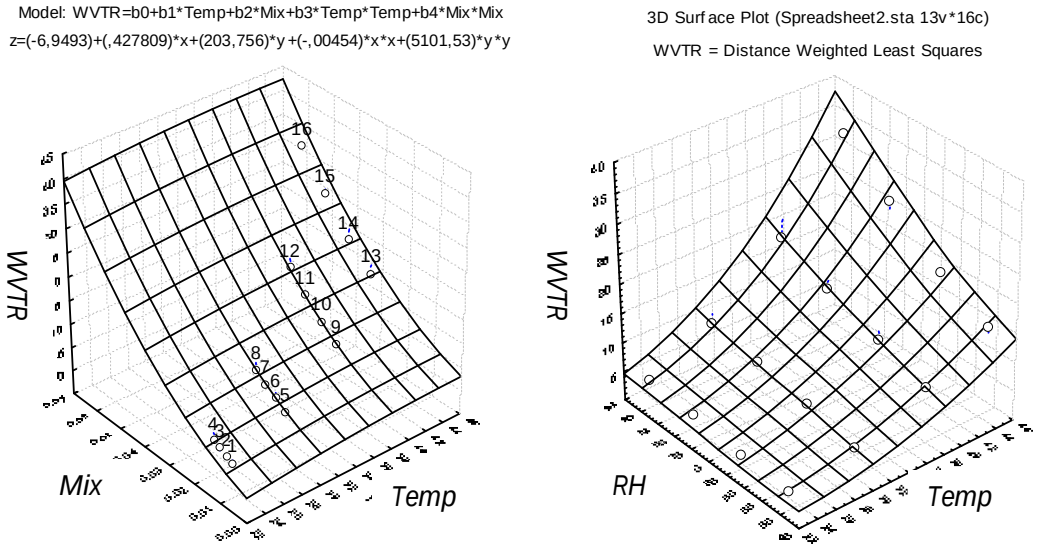

Figure 10. a) a 3-D surface based on the $WVTR_{i,20}(\varpi,T)$ function introducing WVTR of a 20 g/m^2 LDPE-coated paper as a function of mixing ratio and temperature. b) WVTR of a 20 g/m^2 LDPE-coated paper as a function of RH and temperature (distance weighted least squares).

Once all the $WVTR_{i,20}(\varpi,T)$ functions involved are known, one can use Equation (27) for WVTR prediction. The accuracy of this method was tested and proofed in Paper **II**.

4.4. Considerations of accuracy

The purpose of this section is to clarify which diverging factors may cause differences between the measured and predicted WVTR values based on the introduced model. The

most important of these factors, and their influence on WVTR are presented and discussed in following.

4.4.1. Influence of substrate

As discussed in Chapter 2.4, extrusion-coated papers and paperboards are composite materials in which the barrier properties are mainly governed by the coating polymer. Still, the substrate may have a minor influence on the barrier and it may affect indirectly to the coating. With thin coatings, some of the paper fibres may even penetrate the coating completely which clearly reduces the barrier properties of the structure. As the thickness of the coating increases, the barrier effect of fibres will diminish and eventually become insignificant.

In order to investigate the influence of web material on the WVTR of extrusion-coated structures, the WVTRs of two substrates, Lumiflex 90 and Cupforma 280, were measured. 4 parallel measurements were made for both substrates in 23°C and 50% RH conditions. The WVTR results are shown in Table 6 and compared to the WVTRs of PLA and LDPE coated structures taken from earlier investigations. The PLA was coated on Cupforma 210 and the LDPE on Lumiflex 90.

Table 6. WVTR comparison between the extrusion-coated and uncoated structures at 23°C and 50% RH.

	No coating	LDPE 12 g/m^2	LDPE 29 g/m^2	LDPE 8,5 g/m^2	PLA 20 g/m2
Lumiflex 90	500	5,5	2,3		
Cupforma 280	700			10	70*

* Coated on Cupforma 210

The problem in measuring WVTR for web materials is the high permeability level obtained which leads to a rapid saturation and reduced absorption ability of the used calcium chloride. As the saturation of the salt reduces the measured WVTR value, the results tabulated for the web materials in Table 6 should only be considered as suggestive

estimations or minimum values for the exact WVTRs. Still, these estimations can be used in the following comparison.

One way to evaluate the influence of substrate on WVTR is to apply Equation (15) for virtual laminates made of the structures shown in Table 6. Two cases are considered where Lumiflex 90 is laminated on the 12 g/m^2 LDPE coated structure ($WVTR_1$) and Cupforma 280 is laminated on the 8,5 g/m^2 coated board ($WVTR_2$). The WVTRs for these laminates are calculated in Equations (28) and (29).

$$WVTR_1 = \frac{500 * 5{,}5}{500 + 5{,}5} = 5{,}46\,\text{g/m}^2/24\text{h} \approx 99\% \text{ of the original value} \quad (28)$$

$$WVTR_2 = \frac{700 * 10}{700 + 10} = 9{,}86\,\text{g/m}^2/24\text{h} \approx 99\% \text{ of the original value} \quad (29)$$

According to the results, the WVTR improvement provided by the added substrates is extremely small in the considered cases. In conclusion, whenever the structure includes a decent layer (about 10 g/m^2 or more) of LDPE (or better water vapour barrier), the influence of web material on the WVTR is negligible.

In the case of PLA coating, the substrate has greater influence on the WVTR result. $WVTR_3$ and $WVTR_4$ in Equations (30) and (31) represent the water vapour barrier of PLA coated board laminated with Lumiflex 90 and Cupforma 280, respectively.

$$WVTR_3 = \frac{500 * 70}{500 + 70} = 61{,}4\,\text{g/m}^2/24\text{h} \approx 88\% \text{ of the original value} \quad (30)$$

$$WVTR_4 = \frac{700 * 70}{700 + 70} = 63{,}6\ \text{g/m}^2/24\text{h} \approx 91\% \text{ of the original value} \quad (31)$$

In these cases, the WVTR improvement caused by the substrate is considerable despite the substrate has 10 times higher WVTR than the coating. Therefore, the prediction model

should be evaluated individually for each web material when using PLA coatings. Yet, the difference between $WVTR_3$ and $WVTR_4$ is not remarkable as different substrates seem to have a similar effect on the WVTR regardless of the WVTR level of their own. In conclusion, the PLA model based on the use of one web material can be used for common WVTR prediction, but the type of the web should be taken into account in the context of this prediction.

The influence of web materials' fibric surface on the WVTR of coated structures was investigated by performing a pilot-line trial in which LDPE was coated on three substrates, Lumiflex 90, Swanwhite 83 and Cupforma 280. Equal parameters were used with every substrate to obtain three different coating weights, approximately 12, 18 and 35 g/m^2, and nine set points from the trial. Lumiflex 90 that has both pigment-coated and surface-sized surfaces represented a thin and smooth substrate in the test. The non-pigmented side of Lumiflex was extrusion-coated as was done in the modelling. Swanwhite represented a rough but thin substrate in the test, and Cupforma 280 brought the aspect of rough and thick paperboard.

Table 7 shows the WVTR results obtained for the materials and the coating weights measured from the same samples. Tropical conditions (38°C, 90% RH) were used in the WVTR test in order to achieve a significant scatter between the results. Both the coating weights and the WVTRs of the table are mean values of four replicates. One coating weight/WVTR pair (thin coating on Cupforma 280) was neglected from the results due to the obvious error during the WVTR measurement.

Table 7. WVTRs of substrate/LDPE –structures measured in 38°C, 90% RH conditions. Coating weights are shown in parentheses. Unit of WVTR: $g/m^2/24h$, unit of coating weight: g/m^2.

Substrate	WVTR (Coating weight)		
Lumiflex 90	34,7 (11,1)	24,9 (17,2)	12,6 (36,2)
Swanwhite 83	32,9 (12,1)	23,6 (17,1)	11,2 (35,8)
Cupforma 280	30,4 (14,1)	22,7 (19,1)	12,3 (35,2)

In Figure 11, individual coating weight and WVTR results are shown in xy-coordinates together with trendlines based on a power law of regression. According to the figure, no significant difference is found between the barrier levels of the structures that may originate from the web materials. In conclusion, the roughness, porosity and thickness of the web material do not seem to have a considerable influence on WVTR when using common coating thicknesses. Nonetheless, the figure shows that the web materials differ from each other in terms of deviation of the WVTR results. Table 8 shows the standard deviations calculated from the measured coating weight and WVTR values. Regarding the deviation results, the coating weight/WVTR pair neglected from Table 7 is also included in the calculations.

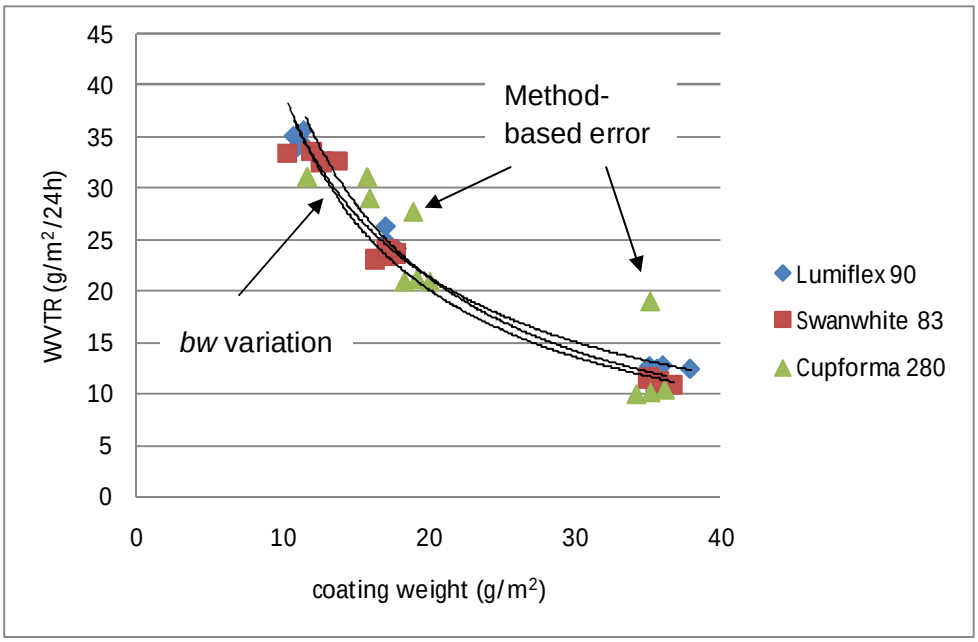

Figure 11. WVTR of substrate/LDPE structures measured in 38°C and 90% RH conditions as a function of coating weight.

Table 8. Standard deviations of the WVTR and coating weight results based on entire populations (analogy with Table 7).

Substrate	Stdev of WVTR (stdev of coating weight)		
Lumiflex 90	0,7 (0,3)	0,9 (0,4)	0,2 (1,1)
Swanwhite 83	0,5 (1,3)	0,4 (0,6)	0,3 (0,6)
Cupforma 280	13,7 (1,8)	3,0 (0,7)	3,9 (0,7)

Table 8 shows clearly the high deviation found for the WVTR results of paperboard samples. Despite of this, the barrier level of the paperboard samples stays comparable with the others. The low deviations obtained with Swanwhite, representing a rough paper, indicate that the loose fibres or porosity of the substrate is not the key factor causing the variation with paperboard. This was also observed from a pinhole test (no pinholes were found from the samples) and microscope images taken from several cross-cut samples (see Figure 12). According to the images, the interface between the web material and the coating was approximately similar with all the tested structures. As an exception, a clearly smoother interface was obtained with the pigment-coated surface of Lumiflex. In conclusion, the deviation experienced with paperboard is not originating from the actual permeation level of the samples. Instead, the possible reasons were sought from the used test method and the basis weight variation of web material.

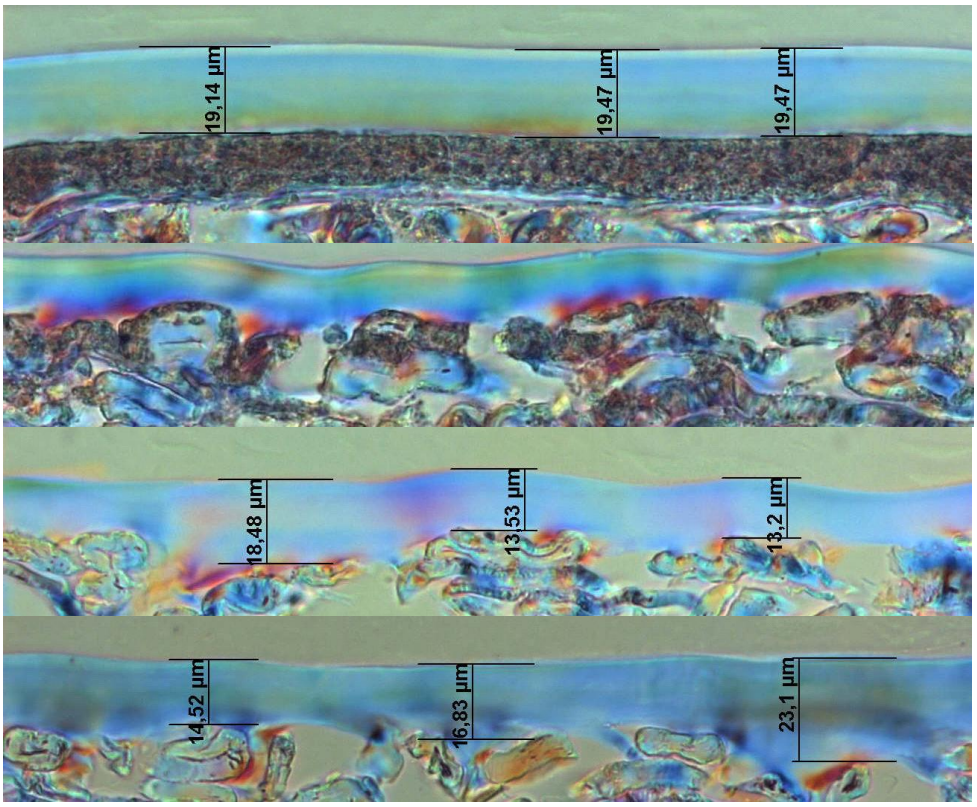

Figure 12. Cross section images from the interface of coated surfaces. The coated surfaces are from top to bottom: Lumiflex (pigment-coated), Lumiflex (reverse side), Swanwhite and Cupforma.

As described in Chapter 3.6, coating weights of the samples were measured by subtracting the influence of web material from the weight result. Therefore, the variation in the basis weight of the substrate is able to cause an error for coating weight results. In order to characterise basis weight variation, 10 basis weight measurements were made for each web material of the test. The samples were drawn from the middle of the roll (cross-direction) approximately 1 m distance from each other. Table 9 shows the average basis weights measured for each web material and the corresponding standard deviations. According to the results, Cupforma's basis weight variation is considerably greater than that of the paper grades. This partially explains the deviation faced with the results of paperboard samples.

Table 9. Average basis weights of the used web materials and their standard deviations.

Substrate	Average basis weight (g/m^2)	Stdev of basis weight (g/m^2)
Lumiflex 90	90,79	0,71
Swanwhite 83	83,33	0,73
Cupforma 280	269,53	1,50

Looking closer to the results of Figure 11, there are two individual WVTR values affected by an error from the WVTR test method. Introducing the WVTR value removed from the figure, three values in total are such cases. Whereas the basis weight variation can be observed as a random error in horizontal direction (Figure 11), the method-based error is observed as individual, clearly increased WVTR-values (vertical direction) far away from a group of lower ones having similar coating weights. The reason for this error was found from the curling of the samples and softening of the wax seam during the WVTR test.

Some paperboard samples sealed on the aluminium dish tend to curl to the coating side when using 38°C or higher temperatures. The softening of the used wax at elevated temperatures assists the stiff paperboard to open the seam which provides an easy entry for water vapour into the cup and increased WVTR value. Presumably, the curling phenomenon originates from the moisture concentration change faced by the paperboard in z-direction /147/. Corresponding behaviour has not been detected with paper samples due to the lower stiffness. Commonly, the dishes with curled sample are neglected from WVTR

results, but sometimes some samples are able to pass the visual inspection as the seam looks to be fine. Also, when an individual WVTR value does not differ too much from the standard level, it is easily accepted among the calculations despite minor, non-visible problems faced by the wax seam. In all probability, this was also experienced with the three samples of the test. In conclusion, it is important to identify and reject the cups with leaking seams when a reliable WVTR value is measured for paperboard samples.

4.4.2. Absorption ability of calcium chloride

The WVTR tests used in the developed model expose each sample to four different atmospheric conditions during a two-week time period (see Table 3). Through this time the calcium chlorine contained by the aluminium dish absorbs all the moisture permeating through the sample. The question is if the absorption ability of calcium chloride stays consistent when the water content of the dish increases towards the end of the period.

The absorption ability of the used calcium chloride was investigated by simulating the series 4 of the standard procedure and measuring the WVTR of four different LDPE-coated structures at 45°C, 90% RH. The first set of samples was exposed to all the four conditions whereas the second set was directly measured at the target conditions. Table 10 shows the conditions used in this test.

Table 10. Conditions used in the absorption ability test.

	1. condition	2. condition	3. condition	4. condition
Series 1	23°C, 90% RH	30°C, 90% RH	38°C, 90% RH	45°C, 90% RH
Series 2	45°C, 90% RH			

Table 11 shows the WVTR results measured for both series at 45°C and 90% RH and the corresponding coating weights (in parenthesis). The results tabulated are mean values of four replicates.

Table 11. WVTR results of absorption ability test measured in 45°C, 90% RH conditions. Coating weights are shown in parentheses.

		WVTR (coating weight) Series 1 at 45°C, 90% RH	WVTR (coating weight) Series 2 at 45°C, 90% RH
Structure 1	Lumiflex 90 / LDPE	57,5 (12,5)	62,3 (11,7)
Structure 2	Lumiflex 90 / LDPE	24,7 (29,4)	25,0 (29,6)
Structure 3	Cupforma 280 / LDPE	55,6 (10,2)	63,0 (10,4)
Structure 4	Cupforma 280 / LDPE	18,2 (36,7)	18,1 (35,6)

According to the table, the coating weights of the samples were more or less equal for both series. Therefore, the influence of absorption ability can be observed from the results. Clear difference between the WVTR results were found for structures 1 and 3. For structures 2 and 4, equal results were obtained from the test. It seems that the WVTRs of the first and third structures were affected by the reduced absorption ability in series 1. This observation was further investigated by calculating the weight increase of the used cups during the whole conditioning period (series 1). The weight increase describes the amount of water absorbed by calcium chloride in each cup. These results are shown in Table 12.

Table 12. Weight increase of the cups in series 1.

	Structure 1	Structure 2	Structure 3	Structure 4
Cup 1	3,2	1,4	4,3	3,2
Cup 2	3,2	1,4	4,0	1,6
Cup 3	3,3	1,4	4,9	5,2
Cup 4	3,4	1,4	4,0	2,8
Average	3,3	1,4	4,3	3,2

Two things can be observed from Table 12. Firstly, the deviation of the weight increase is much higher with paperboard structures. As discussed earlier, random peeling of the wax seams is faced with the dishes holding a paperboard sample. The daily increase of the weight of the dish becomes consistent again when a laboratory assistant repairs the wax seam during the series. Secondly, the absorption ability of calcium chloride starts to decrease and the WVTRs start to fall after about 3 grams of absorbed water. According to the WVTR results, structure 1 had faced the reduced absorption ability whereas structure 4 had not. A closer look at the individual WVTR values caught for structure 4 reveals that the overall level of the results is a bit lower in series 1 than in series 2. In fact, the WVTR result calculated from one cup is able to balance this difference giving equal mean result for

both series. Thus, the amount of absorbed water that starts to affect the absorption ability is somewhere around three grams. However, this quantity cannot be measured accurately because the original water content of the used calcium chloride is not known and the amount of the used salt is not standardised.

The three-gram limit for the weight increase of an individual dish means that the introduced model gives accurate results for about 15 g/m^2 LDPE-coated structures and the barriers better than that. For poorer moisture barriers, the WVTR predictions provided by the model are too low in the case of the most demanding atmospheric conditions. Regarding PLA coatings, the reduced absorption ability of the salt starts to affect the WVTR results already after the first conditions of the series. For PA-6, the method was also found invalid. In a common WVTR test where the sample is put into the controlled atmosphere on Monday and the last weight of the dish is measured on Friday, the three-gram weight increase of the dish equals the WVTR result of about 150 g/m^2/24h.

4.4.3. Both-side-coated webs

Three both-side-coated paper and paperboard structures were produced in order to find out if the developed model is able to predict their WVTRs accurately. In this test, the coated web materials were Lumiflex 90 and Cupforma 280. The coating polymers used were LDPE and HDPE. The coating thicknesses of the samples and the split-ups between top and bottom layers were investigated from cross-cut samples drawn close to the WVTR test samples. The thickness profiles were photographed with a microscope and measured with a standard measuring tool provided by the software. Nine parallel measurements were made for each coating. The unit conversion was made by multiplying the thickness with the density of the coating /121/. The WVTRs tabulated in the results are averages of four parallel measurements. Table 13 shows the coating weights, WVTRs and predicted WVTRs of the studied structures.

Table 13. WVTRs of both-side-coated paper and paperboard structures at 38°C, 90% RH. The results are compared to the predictions given by the developed model.

Structure	Coating weight (g/m^2)	WVTR calculated ($g/m^2/24h$)	WVTR measured ($g/m^2/24h$)
LDPE/paper/LDPE	14,0 + 15,2 = 29,2	15,4	15,3
LDPE/board/LDPE	14,1 + 17,0 = 31,1	16,0	17,4
LDPE/paper/HDPE	11,5 + 24,0 = 35,5	-	12,2
LDPE/paper/HDPE	12,5 + 16,1 = 28,6	13,9	13,3
LDPE/board/HDPE	14,7 + 18,9 = 33,6	12,0	15,0
LDPE/board/HDPE	18,8 + 12,8 = 31,6	11,9	15,8

According to the results, the prediction model seems to estimate logical results for the paper structures, but for the paperboard structures the estimated WVTRs are considerably lower than the measured ones. The explanation for this was not found in the study but it may be caused, e.g., by the two rough paperboard surfaces or by the differences between the first and second extrusion coating processes. This anomalous but interesting outcome requires a more comprehensive study in order to fit the developed model for both-side-coated webs. Thus, the developed model is so far considered not applicable for such materials.

4.5. Statistical model predicting WVTRs for EVOH-coated webs

The statistical model predicting WVTRs of extrusion-coated webs including EVOH-layer is introduced in Paper **III**. It was found that in the case of polar coating polymers, the model developed for non-polar polymers is not applicable. According to the tests made for EVOH- and PA-coated papers, a significant WVTR increase is found in high humidity conditions due to the water sorption of polymer. The rate of this increase is so high that the second-order function (Equation (25)) cannot follow the behaviour of true WVTR. As an example, Figure 13 shows the WVTR graph of 20 g/m^2 EVOH coating as a function of RH and temperature. The figure shows clearly the significant WVTR increase faced by the structure above 70% RH.

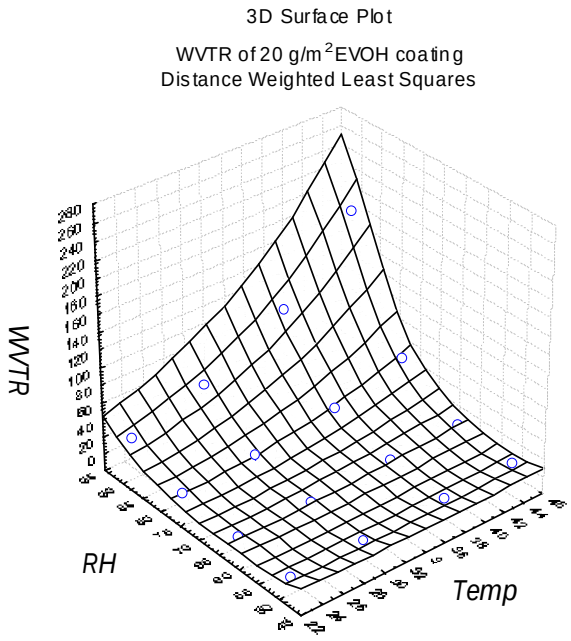

Figure 13. WVTR of a 20 g/m^2 EVOH-coated paper as a function of RH and temperature (distance weighted least squares).

Because of the water sorption of EVOH, the use of atmospheric conditions as input values of the model was found too complex to execute. Therefore, the modelling of this research was focused on the influences of coating structure on WVTR. An accurate fit was found by applying the theory of permeability for multilayer coatings introduced in Chapter 2.4. Unfortunately, this approach could not be executed for the used PA-coating because of the reduced absorption ability of calcium chloride.

Equation (32) shows the WVTR calculation for paper/EVOH/tie/LDPE structure based on the theory of permeability for multilayer structures. As a simplification, the LDPE and adhesive layers are considered as one LDPE layer in the equation. However, it is stated that the theory is valid only if all the permeabilities of the layers are independent of pressure and concentration /11,21/. Clearly, this is not the case with EVOH because of its water sorption. Still, the equation can be modified to obtain accurate prediction. A specific resistance term is introduced into the equation (Equation (33)), which describes how the WVTR of the structure reduces as a function of decreased moisture concentration in EVOH

caused by the LDPE layer (a.k.a. skin layer effect). The resistance term is marked as *R* in Equation (33).

$$WVTR_{tot} = \left(WVTR_{EVOH}{}^{-1} + WVTR_{LDPE}{}^{-1}\right)^{-1} \tag{32}$$

$$WVTR_{tot} = \left(WVTR_{EVOH}{}^{-1} + WVTR_{LDPE}{}^{-1}\right)^{-1} - R \tag{33}$$

The resistance term was calculated for the structure by subtracting the measured WVTR value from the theoretical one based on Equation (32). The average resistance terms calculated for nine different paper/EVOH/tie/LDPE structures in each of the tested 16 atmospheric conditions are shown in Figure 14. According to the figure, the role of the resistance term is found important in high humidity conditions. In mild conditions, the WVTR can be measured accurately without using the resistance term.

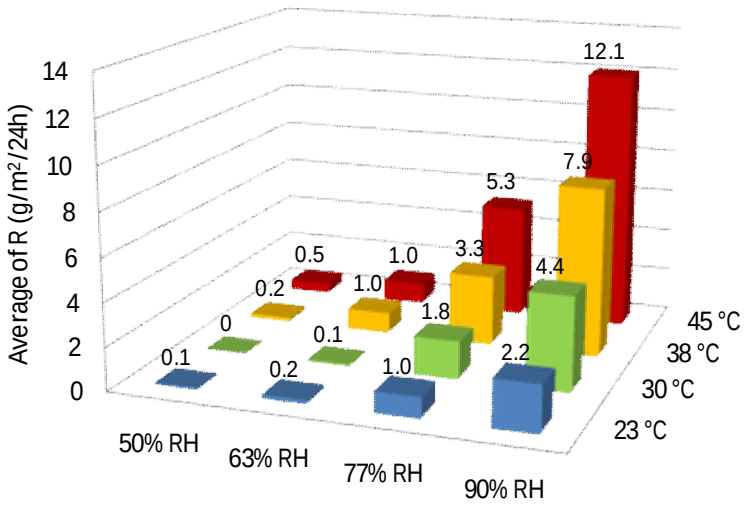

Figure 14. Average resistance terms for paper/EVOH/tie/LDPE structures in various atmospheric conditions.

The behaviour of the resistance term can be modelled statistically. In standard atmospheric conditions, *R* is only a function of basis weights (*bw*) of LDPE and EVOH layers. The best

fit is found with Equation (34) in which the parameters (k_{EVOH}, k_{LDPE}, $k_{EVOH,LDPE}$, A, B and C) are calculated by a statistical software.

$$R = k_{EVOH}\left(bw_{EVOH}\right)^2 + k_{LDPE}\left(bw_{LDPE}\right)^2 + k_{EVOH,LDPE}\left(bw_{EVOH}\right)\left(bw_{LDPE}\right) + A\left(bw_{EVOH}\right) + B\left(bw_{LDPE}\right) + C \quad (34)$$

[**III**, Table 4] shows the resistance function calculated for paper/EVOH/tie/LDPE structure at 38°C, 90% RH conditions. [**III**, Figure 4] shows the corresponding 3-D surface. According to the results, the resistance term seems to find its maximum when using thin LDPE layers of about 10 g/m^2. However, this should not be misjudged to be an optimal situation. The LDPE layer, forming a good moisture barrier by itself, overshadows the importance of the resistance term at high basis weights. In theory, the resistance term is only a part of the EVOH's influence on the total WVTR not participating on the barrier performance of LDPE. Once the resistance term is measured, Equation (33) can be used to predict WVTRs in specific atmospheric conditions.

4.6. Influence of heat treatment on WVTR of polyethylene-coated paper

Typically, the high-rate quenching of extrusion coating process leads to a relatively low density of the coating polymer and reduced barrier properties. Concerning polyethylene-coated papers, it is possible to improve the barrier properties by providing an over-melting-point heat treatment for the structure followed by slow cooling at room temperature. A complete research regarding this phenomenon is introduced in Paper **IV**. Table 14 shows the WVTR- and O_2TR-results obtained for heat-treated 18, 27 and 36 g/m^2 LDPE (CA7230) and 30 g/m^2 HDPE (CG8410) coated papers. The results are further illustrated in Figures 15a and b. The WVTR- and O_2TR-values tabulated are averages of three and two parallel measurements, respectively.

Table 14. WVTR (38°C, 90% RH) and O_2TR (23°C, 0% RH) results for heat-treated LDPE and HDPE coatings.

	LDPE 18 g/m^2		LDPE 27 g/m^2		LDPE 36 g/m^2		HDPE 30 g/m^2	
	WVTR	O_2TR	WVTR	O_2TR	WVTR	O_2TR	WVTR	O_2TR
No treatment	30	13100	22	8000	12	5300	9	1500
130°C 1min	27	10100	14	6400	9	4100	7	1000
5 min	24	9200	14	5400	9	4000	4	500
170°C 1min	21	9600	14	5900	9	3900	5	600
5 min	19	7600	14	5200	9	3500	5	400
210°C 1min	20	7900	14	5200	9	3700	5	500
5 min	26	1300	21	1100	14	1600	over[1]	700

[1] over = over the range of measurement

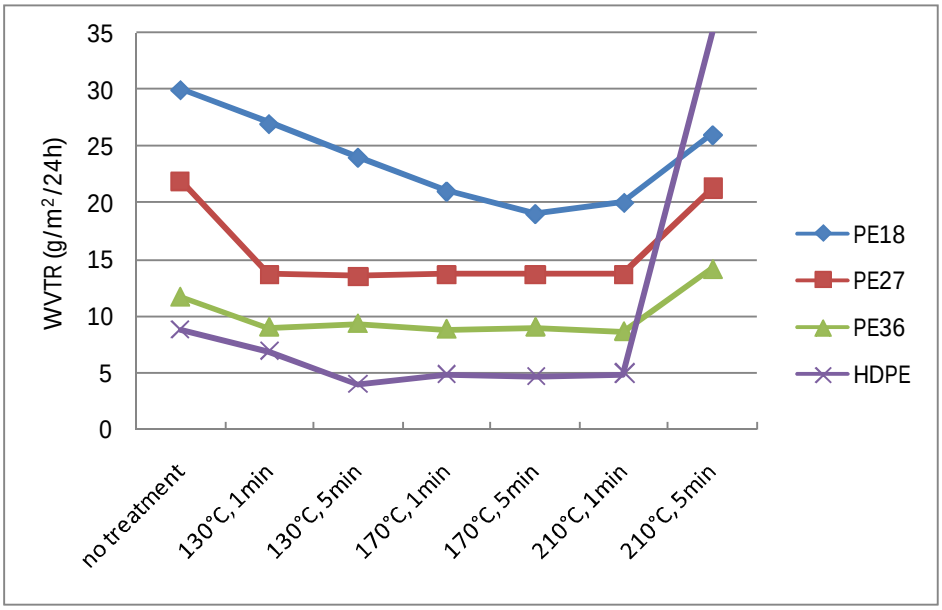

Figure 15a. WVTR (38°C, 90% RH) results of 18, 27 and 36 g/m^2 LDPE and 30 g/m^2 HDPE coatings as a function of heat treatment.

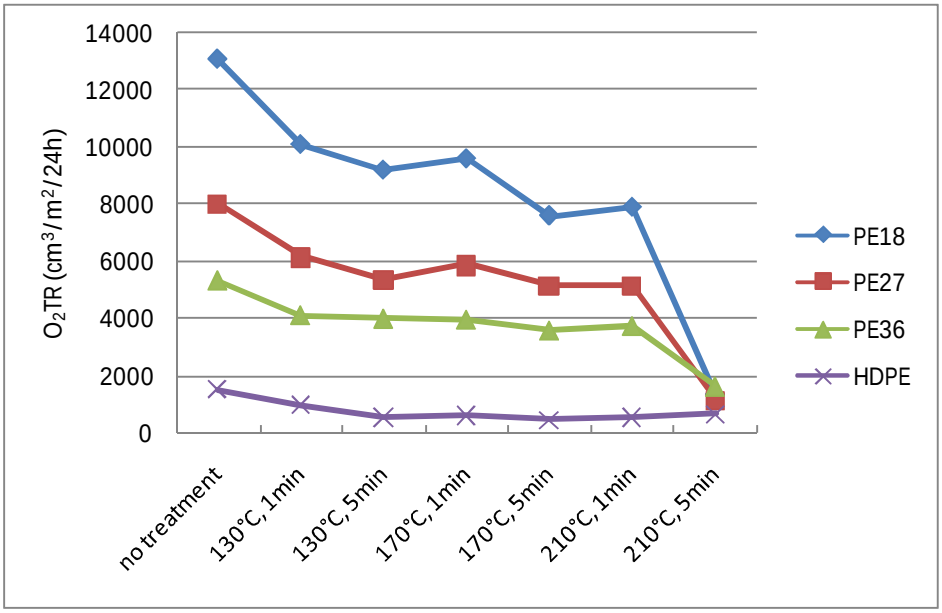

Figure 15b. O_2TR (23°C, 0% RH) results of 18, 27 and 36 g/m^2 LDPE and 30 g/m^2 HDPE coatings as a function of heat treatment.

According to the results, the high-temperature heat treatments considerably decrease the WVTR and O_2TR levels of the samples. It is suggested that the melting of the coating at treatment temperatures followed by the slow cooling allows the polymer layer to reach a significantly higher level of crystallinity and also of higher average diameter of spherulites. These structural changes are able to force the penetrating molecules to a more tortuous path, thereby reducing the transmission rates.

With the 18 g/m^2 coating weight, the WVTR and O_2TR of LDPE decreased linearly following the treatment temperature until 210°C. At this temperature, the 5-minute treatment caused a dramatic decrease in O_2TR obtaining 10 times lower transmission level than the untreated structure. At the same time, the WVTR of the structure faced a corresponding increase but at lower scale. With higher coating weights (27 and 36 g/m^2), the treatment influenced the coatings in a similar manner but the coatings faced a rapid, non-continuous barrier improvement already at 130°C and levelling off above that. Equal behaviour was also found for the HDPE coating. Presumably, the thicker coatings experienced a longer cooling period at room temperature providing extra time for the

crystallisation and packing of the polymer. The dramatic improvement of oxygen barrier at 210°C was also detected for the thicker LDPE coatings but not for HDPE. The 210°C treatment of long period increased also the WVTRs of thicker LDPEs. The water vapour barrier of HDPE coating was even deteriorated at 210°C. Supposedly, easy permeation paths were formed in the structure due to the long-term polymer melting.

Explanations for the significant O_2TR decrease (and for the slight WVTR increase) at 210°C were sought from different directions but the characterisation was not completed thoroughly in Paper **IV**. It was proposed that the reason lies in the larger diameter of the oxygen molecule and its subsequently lower capacity to penetrate through the spherulites of polyethylene comparing to the water molecule. Afterwards, the reasons were also sought from the oxidation of polyethylene.

Figure 16 shows the ATR-IR spectra evaluated for the LDPE-coated samples treated 5 min at 130, 170 and 210°C, and for the untreated sample. According to standard tables /148,149/, the peak at about 1700 cm^{-1} in IR-spectra indicates oxidation of the PE surface (carbonyl groups). It seems that the samples treated at 210°C have experienced significant oxidation comparing to the others. Probably, the small peaks found for the other samples refer to the air-gap oxidation at the extrusion coating process. It can be suggested that the significant oxidation of LDPE led to intermolecular bonding at the surface areas of the coating followed by restricted chain mobility and improved oxygen barrier properties. At the same time, the enhanced water sorption of the surface caused the slightly increased WVTR level. On the other hand, the O_2TR decrease was not found for HDPE because of its ultimately lower transmission level. Still, these suggestions should not be considered as proofed facts.

Influences of heat treatments on other functional properties of PE were also investigated in this research. Curling properties, optical characteristics, heat sealability and surface energies of the heat-treated samples were tested. The results and discussion regarding these tests are shown in Paper **IV**.

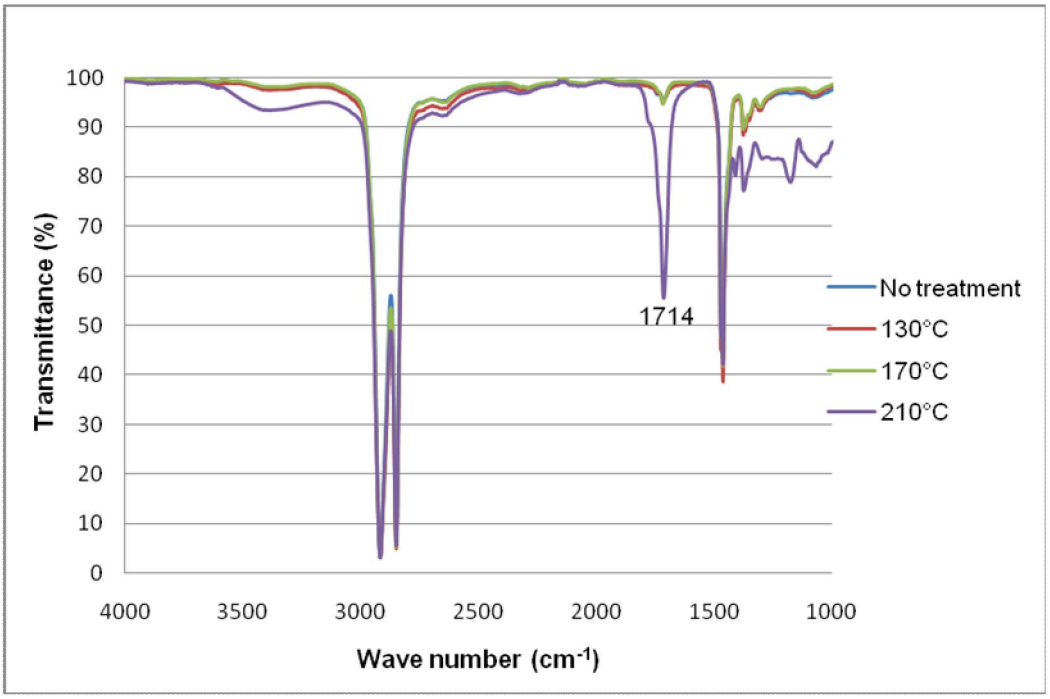

Figure 16. ATR-IR spectra evaluated for LDPE coatings heat-treated 5 min at specific temperatures.

4.7. Influence of heat treatment on WVTR of polylactide-coated paperboard

In Paper **V**, heat treatments were used to improve the water vapour barrier properties of polylactide-coated paperboard. The performed treatments yielded the temperatures from 100 to 150°C, not exceeding above the melting temperature of PLA, and periods from 2 to 40 min. Table 15 shows the WVTR results obtained for 20 g/m^2 PLA-coated structures. In the test, the measuring conditions were 23°C, 50% RH. The results tabulated in the table are mean values of four replicates. The results are further illustrated and compared to the WVTR on untreated structure (74 g/m^2/24h) in Figure 17.

Table 15. WVTRs of 20 g/m^2 PLA-coated paperboard samples as a function of time and temperature of the heat treatment; unit of the WVTR: g/m^2/24h; measuring conditions: 23°C, 50% RH.

	100 °C	110 °C	120 °C	130 °C	140 °C	150 °C
2 min	84	81	87	74	66	52
5 min	75	78	73	63	54	47
10 min	70	61	55	54	51	38
20 min	58	52	42	39	43	36
40 min	61	49	45	31	43	41

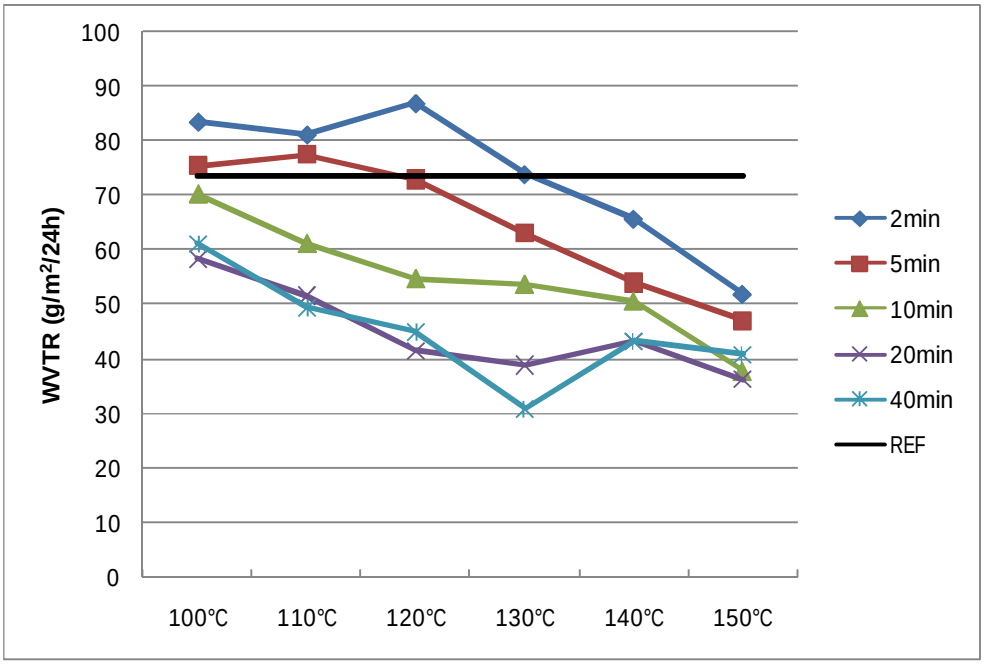

Figure 17. WVTRs of 20 g/m^2 PLA-coated samples as a function of time (colour) and temperature (x-axis) of the heat treatment. Measuring conditions: 23°C, 50% RH. The straight line shows the WVTR of the untreated structure.

According to the results, the heat treatments are able to decrease the WVTR of PLA-coated paperboard considerably. The greatest barrier improvement was found after 20 min heating. Further improvement was not detected by extending the treatment period. As an exception, the lowest WVTR of the series (31 g/m^2/24h) was found after a 40 min treatment at 130°C.

In order to find reasons for improved WVTR, the PLA matrices were studied from cross-cut images taken by an optical microscope. The images of the samples after long-duration treatments at 110, 130 and 150°C are shown in [**V**, Figure 2]. The images show that the

coatings exposed to 110 and 130°C include a considerable amount of crystalline spherulites whereas the coating treated at 150 °C does not. According to Yuryev et al. /150/, the fastest crystalline growth for poly-D,L-lactide is found at around 120-130°C. At higher temperatures, the crystalline growth is not found, which indicates that the PLA coatings treated at 140-150°C have remained more or less amorphous. The cross-section images of [**V**, Figure 2] support this suggestion.

The morphologies of the heat-treated PLA samples were further investigated from the IR-spectra taken directly from the surface of the coating. [**V**, Figure 4] shows the IR spectra evaluated from the samples treated for 20 min at 100-150°C and from an untreated sample. According to the spectra, crystals were found in the samples treated at 100-130°C. The highest crystalline growth was achieved at 110 and 120°C. As suggested, the treatments at 140 and 150°C did not cause any crystallisation for PLA. The DSC measurements performed showed also the crystalline growth in PLA at 100-130°C. Unfortunately, DSC measurements could not be made with the samples treated at 140-150°C because of the very good adhesion formed between the web material and the coating.

In conclusion, the heat treatments accumulated two kinds of reordering mechanisms in PLA resulting in better barrier performance. The treatments at 100-130°C provided a crystalline growth in the originally amorphous PLA resulting in a more tortuous path for moisture to penetrate through the coating. Because the WVTR levels of the samples decreased also after the treatments at 140-150°C, the treatments also altered the amorphous section of the PLA matrix. The reordering of the amorphous section decreased the WVTR level of the samples even more than the crystallisation. It was suggested that the lowest WVTR was achieved after a 40 min treatment at 130°C because it efficiently accumulated both reordering mechanisms for PLA: the crystalline growth and the packing of the amorphous section.

The effects of heat treatments on heat sealability of PLA-coated paperboard were also tested in this research. The results regarding this test are shown and discussed in Paper **V**.

5. CONCLUSIONS

Paper **I** introduced a practical exponential function that can be used to estimate WVTRs of extrusion-coated papers as a function of coating weight in specific atmospheric conditions. The correlations between WVTR and the absolute humidity of surroundings were also studied. A strong linear correlation was found between the variables when using non-polar coating polymers. The change in temperature influenced mainly on the slope of the straight WVTR vs. absolute humidity curve showing the role of activation energy of diffusion and heat of solution in the permeabilities of the studied structures.

Paper **II** used regression analysis and the previously found WVTR-humidity correlation to create a statistical prediction model for WVTR that takes into account all the external factors affecting water vapour permeation, i.e. temperature and moisture concentration of surroundings, and the layer profile of a multilayer coating. This model formed a practical and accurate tool for WVTR prediction, and is already available for laboratories /151/.

The research introduced in Paper **III** was aimed at expanding the Paper **II** model for the structures including a polar EVOH layer. As the WVTR-humidity correlation was found too complex, the investigations were focused on the resistance effect caused by a non-polar skin layer on the moisture absorption of EVOH and the WVTR improvement obtained because of it. The study showed the importance of the resistance effect in high humidity conditions and introduced a statistical model that predicts the resistance term as a function of basis weights of the EVOH and skin layers. Once the resistance term is measured, the theory of permeability for multilayer structures provides an accurate WVTR prediction.

Paper **IV** studied the influences of high-temperature heat treatments on WVTR and O_2TR of LDPE and HDPE coated paper, and showed that considerable improvements can be found. By heating the coatings up to 130-210°C followed by free cooling at room temperature, the WVTR and O_2TR of LDPE and HDPE decreased most likely as a consequence of morphology changes. After 210°C, the treatment caused a dramatic O_2TR decrease for LDPE, achieving about 10 times lower values than untreated structure. At the

same time, the WVTR faced a corresponding increase but at a lower scale. The reasons for these phenomena were sought from the difference in penetrant size (H_2O and O_2 molecules), and from the oxidation of the polymer.

Paper **V** studied the water vapour barrier properties of heat-treated, PLA extrusion-coated paperboard. It was found that PLA experienced crystalline growth at 100-130°C temperatures. At higher temperatures (up to 150°C), the crystalline growth did not occur, but the PLA faced packing of the amorphous section which was found to be the decisive factor affecting WVTR. The greatest barrier improvement (about 2,5 times lower WVTR than that of the untreated structure) was found after a 40 min treatment at 130°C. Most likely, this treatment accumulated both reordering mechanisms for PLA.

In order to support the findings of this study, further investigations are recommended in the following list. One could

- perform a more detailed study over the WVTR of both-side-coated webs,
- investigate the fit of two-phase models for the WVTR of EVOH-coated papers (separate formulae for low and high humidity conditions),
- harmonise the created models with the other test methods than SCAN P22:68,
- study in detail the effects of over 200°C heat treatments on polyolefins and
- investigate the effects of heat treatments on the amorphous section of PLA.

REFERENCE

1. Brown H and Williams J. Chapter 3 in: Coles, McDowell, Kirwan (eds) *Food Packaging Technology*. Blackwell Publishing. Great Britain 2003.
2. Troedel M. *Tappi 1999 Polymers, Laminations and Coatings Conference*. Atlanta, GA. 22-26 Aug 1999.
3. Mercea P. Chapter 5 in: Piringer, Baner (eds) *Plastic Packaging Materials for Food*. Wiley-VCH. Germany 2000.
4. Chainey M. Chapter 11 in: Cheremisinoff (ed) *Handbook of Polymer Science and Technology, Vol 4*. Marcel Dekker. USA 1989.
5. Wm. Tock R. *Adv. Polym. Tech.* **3** (1983) 223.
6. Koros W. *Tappi 2002 PLACE Conference*. Boston, MA. 9-12 Sep 2002.
7. Yasuda H, Clark H and Stannett V. "Permeability" In: Mark, Gaylord (eds) *Encyclopedia of Polymer Science and Technology, Vol 9*. John Wiley & Sons. USA 1968.
8. Yasuda H. *J. Appl. Polym. Sci.* **19** (1975) 2529.
9. Frisch H. *J. Phys. Chem.* **60** (1956) 1177.
10. Kuusipalo J. *PHB/V in Extrusion Coating of Paper and Paperboard*. Doctoral Thesis. Tampere University of Technology. Finland 1997.
11. Stannett V, Szwarc M, Bhargava R, Meyer J, Myers A and Rogers C. *Permeability of Plastic Films and Coated Papers.* Tappi Monograph No. 23. USA 1962.
12. DeLassus P. "Barrier Polymers" In: Kroschwitz J, Howe-Grand (eds) *Kirk-Othmer Encyclopedia of Chemical Technology, Vol 3*. John Wiley & Sons. Canada 1992.
13. Combellick W. "Barrier Polymers" In: Mark, Bikales, Overberger, Menges, Kroschwitz (eds) *Encyclopedia of Polymer Science and Engineering, Vol 2*. John Wiley & Sons. Canada 1985.
14. Naylor T. Chapter 20 in: Allen, Bevington (eds) *Comprehensive Polymer Science, Vol 2*. Pergamon Press. Great Britain 1989.
15. Vieth W. 1991. *Diffusion In and Through Polymers, Principles and Applications*. Hanser Publishers. Germany 1991.

16. Nemphos S, Salame M and Steingiser S. “Barrier Polymers” In: Mark, Bikales (eds) *Encyclopedia of Polymer Science and Technology, Vol 1*. John Wiley & Sons. Canada 1976.
17. ASTM-E 96. *Standard Test Methods for Water Vapor Transmission of Materials*. ASTM International. USA 2005.
18. Salame M. “Barrier Polymers” In: Bakker, Eckroth (eds) *The Wiley Encyclopedia of Packaging Technology*. John Wiley & Sons. Canada 1986.
19. Salame M and Steingiser S. *Polym-Plast. Tech. Eng*. **8** (1977) 155.
20. Zhang Z, Britt I and Tung M. *J. Appl. Polym. Sci.* **82** (2001) 1866.
21. Yasuda H and Stannett V. “Barriers, Vapor” In: Mark, Bikales (eds) *Encyclopedia of Polymer Science and Technology, Vol 2*. John Wiley & Sons. Canada 1976.
22. Vieth W, Howell J and Hsieh J. *J. Membrane Sci.* **1** (1976) 177.
23. Frisch H and Stern S. “Diffusion of Small Molecules in Polymers”. *CRC Crit. Rev. Solid State and Materials Sci*. **11** (1983) 123.
24. Stannett V, Koros W, Paul D, Lonsdale H and Baker R. *Adv. Polym. Sci.* **32** (1979) 71.
25. Paul D and Koros W. *J. Polym. Sci: Polym. Phys. Ed*. **14** (1976) 675.
26. Stern S and Saxena V. *J. Membrane Sci.* **7** (1980) 47.
27. Saxena V and Stern S. *J. Membrane Sci.* **12** (1982) 65.
28. Barrer R. *Trans. Faraday Soc*. **35** (1939) 262 & 644.
29. Barrer R. *Trans. Faraday Soc*. **38** (1942) 321.
30. Meares P. *J. Am. Chem. Soc*. **76** (1954) 3415.
31. Meares P. *Eur. Polym. J*. **29** (1993) 237.
32. Brandt W. *J. Phys. Chem.* **63** (1959) 1080.
33. DiBenetto A. *J. Polym. Sci.* **A1** (1963) 3459.
34. DiBenetto A. *J. Polym. Sci.* **A1** (1963) 3477.
35. Pace R and Datyner A. *J. Polym. Sci: Polym. Phys. Ed*. **17** (1979) 437.
36. Pace R and Datyner A. *J. Polym. Sci: Polym. Phys. Ed*. **17** (1979) 453.
37. Pace R and Datyner A. *J. Polym. Sci: Polym. Phys. Ed*. **17** (1979) 465.
38. Chandrasekar S. *Rev. Mod. Phys*. **15** (1943) 1.
39. Cohen M and Turnbull *J. Chem. Phys*. **31** (1959) 1164.

40. Vrentas J, Duda J and Ling H. *Macromolecules*. **21** (1988) 1470.
41. Vrentas J, Duda J, Ling H and Hou A. *J. Polym. Sci: Polym. Phys. Ed*. **23** (1985) 275 & 289.
42. Vrentas J and Vrentas C. *Macromolecules*. **27** (1994) 4684.
43. Vrentas J, Duda J and Hou A. *J. Appl. Polym. Sci*. **33** (1987) 2581.
44. Vrentas J and Vrentas C. *Macromolecules*. **27** (1994) 5570.
45. Vrentas J, Duda J and Ling H. *J. Appl. Polym. Sci*. **42** (1991) 1931.
46. Vrentas J and Duda J. *J. Polym. Sci: Polym. Phys. Ed*. **15** (1977) 403.
47. Vrentas J and Duda J. *J. Polym. Sci: Polym. Phys. Ed*. **15** (1977) 417.
48. Vrentas J and Duda J. *J. Polym. Sci: Polym. Phys. Ed*. **15** (1977) 441.
49. Vrentas J and Duda J. *J. Appl. Polym. Sci*. **21** (1977) 1715.
50. Vrentas J and Duda J. *J. Appl. Polym. Sci*. **22** (1978) 2325.
51. Frisch H. *Polym. Eng. Sci*. **20** (1980) 2.
52. Barrer R, Barrie J and Slater J. *J. Polym. Sci*. **27** (1958) 177.
53. Petropoulos J. *J. Polym. Sci.* **A-2, 8** (1970) 1797.
54. Tshudy J and von Frankenberg C. *J. Polym. Sci.* **A-2, 11** (1973) 2077.
55. Crank J. *Mathematics of Diffusion*. Claredon Press. Great Britain 1975.
56. Wang T, Kwei K and Frisch H. *J. Polym. Sci*. **A-2, 7** (1969) 879.
57. Fredrickson G and Helfand E. *Macromolecules*. **18** (1985) 2201.
58. Vieth W and Sladek K *J. Colloid Sci.* **20** (1965) 1014.
59. Stern S. *J. Membrane Sci.* **94** (1994) 1.
60. Vrentas J, Duda J and Ling H. *J. Polym. Sci: Polym. Phys. Ed*. **26** (1988) 1059.
61. Vrentas J, Vrentas C. *J. Polym. Sci: Polym. Phys. Ed*. **30** (1992) 1005.
62. Vrentas J, Liu H and Duda J. *J. Appl. Polym. Sci*. **25** (1980) 1297.
63. Catlow C, Parker S and Allen M (eds) *Computer Modelling of Fluids, Polymers and Solids*. Kluwer. Netherlands 1990.
64. Roe R. *Computer Simulations of Polymers*. Prentince Hall. USA 1991.
65. Gusev A, Müller-Plathe F, van Gunsteren W and Suter U. *Adv. Polym. Sci.* **116** (1993) 207.
66. Müller-Plathe F. *Acta Polymerica*. **45** (1994) 259.

67. Theodorou N. Chapter 2 in: Neogi (ed) *Diffusion in Polymers*. Marcel Dekker. USA 1996.
68. Gusev A, Arizzi S, Suter U and Moll D. *J. Chem. Phys*. **99** (1993) 2221.
69. Gusev A and Suter U. *Polym. Preprints.* **16** (1992) 631.
70. Gusev A and Suter U. *Macromol Chem: Macromol. Symp*. **69** (1993) 229.
71. Gusev A and Suter U. *J. Chem. Phys*. **99** (1993) 2228.
72. Müller-Plathe F. *Chem. Phys. Lett*. **177** (1991) 527.
73. Takeuchi H. *J. Chem. Phys*. **93** (1990) 2062 & 4490.
74. Fritz L and Hofmann D. *Polymer*. **38** (1997) 1035.
75. Hofmann D, Fritz L, Ulbrich J and Paul D. *Polymer*. **38** (1997) 6145.
76. Jakobsen M and Risbo J. *Packag. Technol. Sci*. **21** (2008) 207.
77. Howsmon G and Peppas N. *J. Appl. Polym. Sci.* **31** (1986) 2071.
78. Hedenqvist M and Gedde U. *Packag. Technol. Sci*. **12** (1999) 131.
79. Ritums J, Neway B, Doghieri F, Bergman G, Gedde U and Hedenqvist M. *J. Polym. Sci. B Polym. Phys.* **45** (2007) 723.
80. Lee W. *Polym. Eng. Sci*. **20** (1980) 65.
81. Del Nobile M, Buonocore G, Dainelli D and Nicolais L. *J. Food Sci.* **69** (2004) 85.
82. Peppas N and Khanna R. *Polym. Eng. Sci.* **20** (1980) 1147.
83. Smith J and Peppas N. *J. Appl. Polym. Sci*. **43** (1991) 1219.
84. Stroeks A and Dijkstra K. *Polymer*. **42** (2001) 117.
85. Lange J, Büsing B, Hertlein J and Hediger S. *Packag. Technol. Sci*. **13** (2000) 139.
86. Marsh K. *Tappi Polymers, Laminations and Coatings Conference*. Boston, MA. 24-26 Sep 1984.
87. Risbo J. *J. Food Eng.* **58** (2003) 239.
88. Tanner D, Cleland A and Robertson T. *Int'l J. Refriger*. **25** (2002) 54.
89. Azanha A and Faria J. *Packag. Technol. Sci.* **18** (2005) 171.
90. Pfeiffer C, D'Aujourd'Hui M, Walter J, Nuessli J and Escher F. *Food Tech*. **53** No.6 (1999) 52.
91. Laragon J, Catalá R and Gavara R. *Mater. Sci. Tech*. **20** (2004) 1.
92. Boyd R. *Polym. Eng. Sci*. **19** (1979) 1010.

93. Hedenqvist M, Angelstok A, Edsberg L, Larsson P and Gedde U. *Polymer*. **37** (1996) 2887.
94. Liu R, Schiraldi D, Hiltner A and Baer E. *J. Polym. Sci. B Polym. Phys*. **40** (2002) 862.
95. Dosière M. Chapter 12 in: Cheremisinoff (ed) *Handbook of Polymer Science and Technology, Vol 2*. Marcel Dekker. USA 1989.
96. Lustiger A, Lotz B and Duff T. *J. Polym. Sci. B Polym. Phys*. **27** (1989) 561.
97. Keith H and Padden Jr F. *J. Polym. Sci. B Polym. Phys*. **25** (1987) 2371.
98. Al-Raheil I and Al-Sharé M. *J. Appl. Polym. Sci*. **72** (1999) 1125.
99. Neway B. *The Influence of Morphology on the Transport and Mechanical Properties of Polyethylene*. Doctoral Thesis. Royal Institute of Technology. Sweden 2003.
100. Neway B, Hedenqvist M and Gedde U. *Polymer*. **44** (2003) 4003.
101. Magoń A and Pyda M. *Polymer*. **50** (2009) 3967.
102. Tsuji H, Okino R, Daimon H and Fujie K. *J. Appl. Polym. Sci*. **99** (2006) 2245.
103. Rhim J, Lee J and Hong S. *Packag. Technol. Sci*. **20** (2007) 393.
104. Drieskens M, Peeters R, Mullens J, Franco D, Lemstra P and Hristova-Bogaerds D. *J. Polym. Sci. B Polym. Phys.* **47** (2009) 2247.
105. Qin Y, Rubino M and Auras R. *Tappi 2006 PLACE Conference*. Cincinnati, OH. 17-21 Sep 2006.
106. Billham M, Millar B, McNally G and Murphy W. *ANTEC 2005*. Boston, MA. 1-5 May 2005. Pgs. 2942-2946.
107. Edwards R. Chapter 18 in: Bezigian (ed) *Extrusion Coating Manual*. Tappi Press. USA 1999.
108. Fischer E. *Pure Appl. Chem*. **31** (1972) 113.
109. Keller A and O'Connor A. *Disc. Faraday Soc*. **24** (1958) 114.
110. Statton W and Geil P. *J Appl. Polym. Sci*. **3** (1960) 357.
111. Edwards R. Chapter 19 in: Bezigian (ed) *Extrusion Coating Manual*. Tappi Press. USA 1999.
112. Tuominen M, Vähä-Nissi M and Kuusipalo J. Chapter 2 in: Kuusipalo (ed) *Paper and Paperboard Converting*. Finnish Paper Engineers' Association. Finland 2008.

113. Hartmann M. *ANTEC 2001*. Dallas, TX. 6-10 May 2001. Pgs. 2-6.
114. De Candia F, Russo R, Vittoria V and Peterlin A. *J Polym. Sci: Polym. Phys. Ed*. **18** (1980) 2083.
115. Yu L, Liu H, Xie F, Chen L and Li X. *Polym. Eng. Sci.* **48** (2008) 634.
116. Stora Enso. Flexible Packaging Papers. LumiFlex – Technical Data Sheet. Dec 2003.
117. UPM-Kymmene. Wisapaper. UPM SwanWhite – Technical Data Sheet. 26 Mar 2003.
118. Stora Enso. Consumer Board. Cupforma Classic – Technical Data Sheet. Mar 2002.
119. ISO 8791-3. *Paper and board – Determination of roughness/smoothness (air leak methods)*. International Organization for Standardization. USA 2005.
120. Borealis. Solutions for extrusion coating applications – Data Sheet. 2007.
121. Borealis. *Polyolefins for Extrusion Coating*, 2nd Ed. – Booklet. Austria 2008.
122. Topas Advanced Polymers. Topas 8007F-400 – Technical Data Sheet. 30 May 2006.
123. EVAL Europe. EVAL F104B – Technical Data Sheet. 17 Jul 2008.
124. BASF. Ultramid B27 E – Technical Data Sheet. Sep 2008.
125. EMS. Grilon F 28 – Technical Data Sheet. Jun 2003.
126. DuPont. Bynel resins – Product Data Sheet. 22 Feb 2007.
127. Kuusipalo J, Savolainen A, Laiho E and Penttinen T. Chapter 4 in: Kuusipalo (ed) *Paper and Paperboard Converting*. Finnish Paper Engineers' Association. Finland 2008.
128. Kirwan M. Chapter 8 in: Coles, McDowell, Kirwan (eds) *Food Packaging Technology*. Blackwell Publishing. Great Britain 2003.
129. Jester R. *Tappi 2005 PLACE Conference*. Las Vegas, NV. 27-29 Sep 2005.
130. Goerlitz W. *Tappi 8th European Polymers, Films, Laminations and Extrusion Coatings Conference*. Barcelona, Spain. 28-30 May 2001.
131. Topas Advanced Polymers. Packaging - brochure. Germany 2007.
132. Armstrong R. *Tappi 2002 PLACE Conference*. Boston, MA. 9-12 Sep 2002.
133. Torradas J. *Tappi 2006 PLACE Conference*. Cincinnati, OH. 17-21 Sep 2006.
134. Gregory B. *Extrusion Coating: A Process Manual*. Trafford Publishing. USA 2007.

135. Yasui S. *Tappi Innovations in Barrier Packaging Symposium*. Atlanta, GA. 7-8 Jun 2006.
136. Giles H, Wagner Jr. J and Mount III E. *Extrusion – The Definitive Processing Guide and Handbook, Part 6: Coextrusion*. William Andrew Publishing/Plastics Design Library. USA 2005.
137. Kelly W. *Tappi Innovations in Barrier Packaging Symposium.* Atlanta, GA. 7-8 Jun 2006.
138. Drumright R, Gruber P and Henton D. *Adv. Mater.* **12** (2000) 1841.
139. Auras R, Harte B and Selke S. *Macromol. Biosci.* **4** (2004) 835.
140. Komatsuka T, Kusakabe A and Nagai K. *Desalination*. **234** (2008) 212.
141. Auras R, Harte B and Selke S. *J. Appl. Polym. Sci*. **92** (2004) 1790.
142. Lehermeier H, Dorgan J and Way D. *J. Membrane Sci.* **190** (2001) 243.
143. SCAN P22:68. *Paperin ja kartongin vesihöyryn läpäisevyys*. Scandinavian Pulp, Paper and Board Testing Committee. Finland 1967.
144. ASTM-D 5946. *Standard Test Method for Corona-Treated Polymer Film Using Water Contact Angle Measurements*. ASTM International. USA 1999.
145. Keenan J. *Thermodynamics*. John Wiley & Sons. USA 1957.
146. Fagerholm N. *Termodynamiikka*. Gummerus Oy. Finland 1986.
147. Kajanto I and Niskanen K. Chapter 7 in: Niskanen (ed) *Paper Physics*. Fapet Oy. Finland 1998.
148. Williams D and Fleming I. *Spectroscopic methods in organic chemistry*. McGraw-Hill. United Kingdom 1989.
149. Yang R, Liu Y, Yu J and Wang K. *Polym. Degrad. Stab*. **91** (2006) 1651.
150. Yuryev Y, Wood-Adams P, Heuzey M, Dubois C and Brisson J. *Polymer*. **49** (2008) 2306.
151. Lahtinen K and Kuusipalo J. *Tappi 2008 PLACE Conference*. Portsmouth, VA. 14-17 Sep 2008.

APPENDIX 1

KOSTEA ILMA h, ω PIIRROS LIITE 9

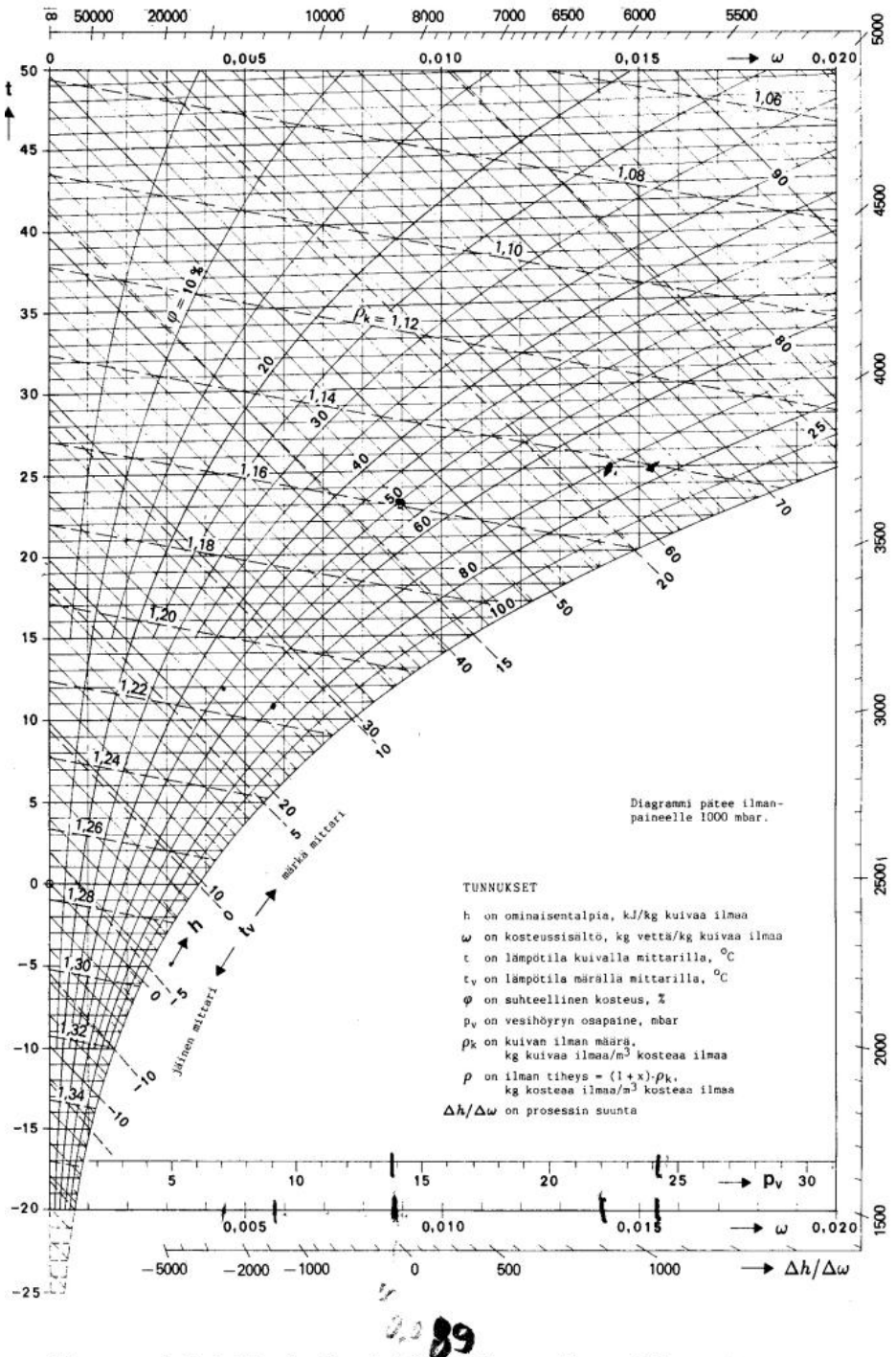

Diagrammi: Puhallintekniikan käsikirja, Ilmateollisuus OY

372

Paper I

Influence of Temperature and Mixing Ratio on Water Vapor Barrier Properties of Extrusion-Coated Paper

Jurkka Kuusipalo and Kimmo Lahtinen

Int'l J. Polym. Anal. Charact. **2005**, Vol. 10, Issue 1-2, Pgs. 71-83.

Paper II

Statistical prediction model for water vapor barrier of extrusion-coated paper

Kimmo Lahtinen and Jurkka Kuusipalo

Tappi J. **2008**, Vol. 7, Issue 9, Pgs. 8-15.

Paper III

Statistical Model Predicting Water Vapor Transmission Rates of High-Barrier-Coated Papers

Kimmo Lahtinen and Jurkka Kuusipalo

ANTEC 2009 – Proceedings of the 67th Annual Technical Conference & Exhibition, Chicago, IL, June 22-24, Society of Plastics Engineers, Pgs. 220-224.

Paper IV

Influence of High-Temperature Heat Treatment on Barrier and Functional Properties of Polyolefin-Coated Papers

Kimmo Lahtinen, Kalle Nättinen and Jari Vartiainen

Polym-Plast. Tech. Eng. **2009**, Vol. 48, Issue 5, Pgs. 561-569.

Paper V

Characterization for Water Vapour Barrier and Heat Sealability Properties of Heat-Treated Paperboard/Polylactide Structure

Kimmo Lahtinen, Sami Kotkamo, Tapio Koskinen, Sanna Auvinen and Jurkka Kuusipalo

Packag. Technol. Sci. **2009**, Vol. 22, Issue 8, Pgs. 451-460.
